2019 Fall

"Advanced Physical Metallurgy"

- Non-equilibrium Solidification -

11.25.2019

Eun Soo Park

Office: 33-313
Telephone: 880-7221
Email: espark@snu.ac.kr
Office hours: by appointment

5 Crystallization Behavior

Crystallization to Equilibrium or Non-equilibrium Phase.

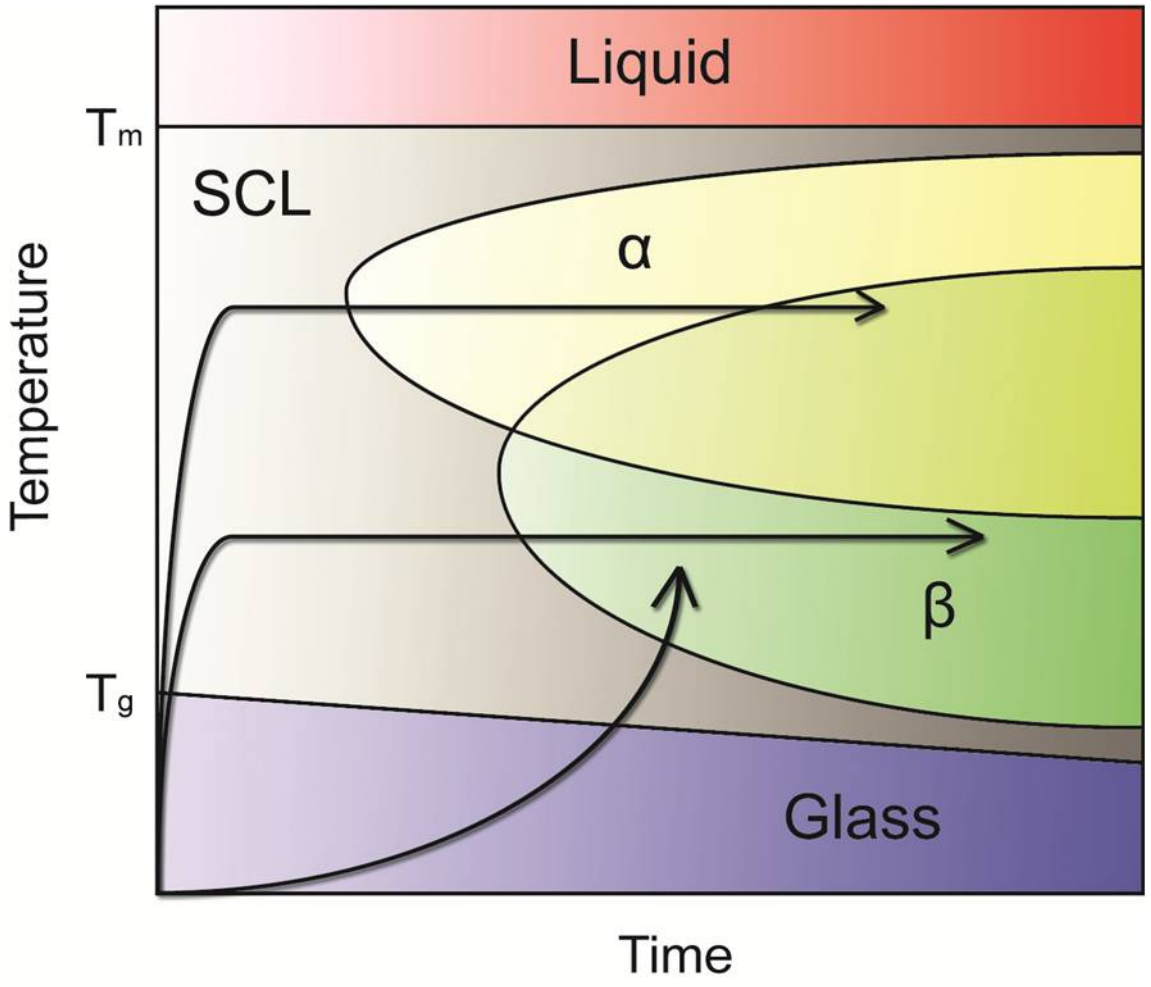

α : Equilibrium phase

β : Non-Equilibrium phase

Cooling Process.

Only α phase

Heating Process.

Low T Crystallize to β

High T Crystallize to α

Science

AAAS

Beating Crystallization in Glass-Forming Metals by Millisecond Heating and Processing

William L. Johnson *et al.*

Science **332**, 828 (2011);

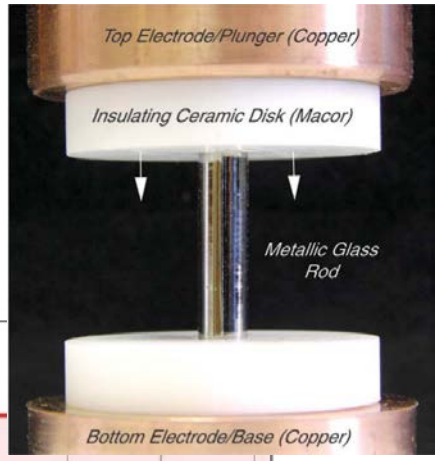

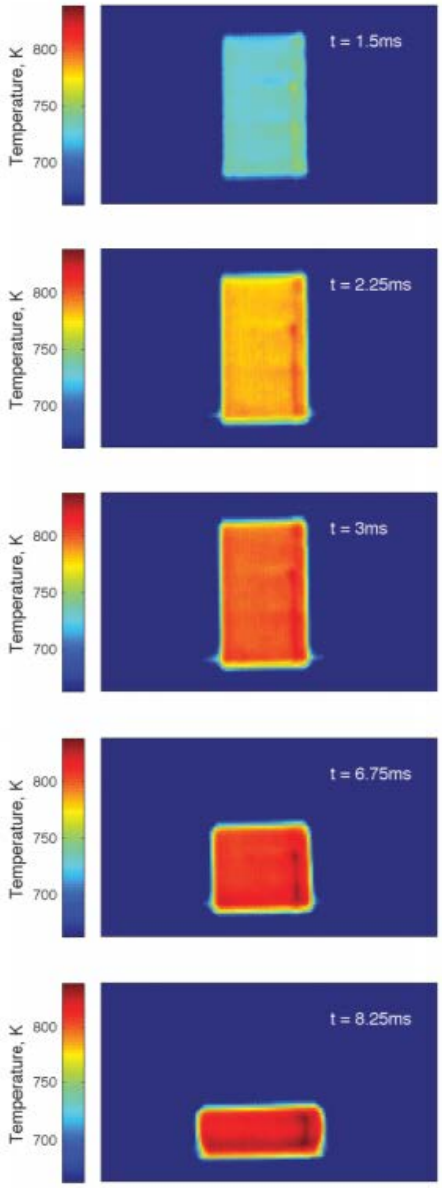

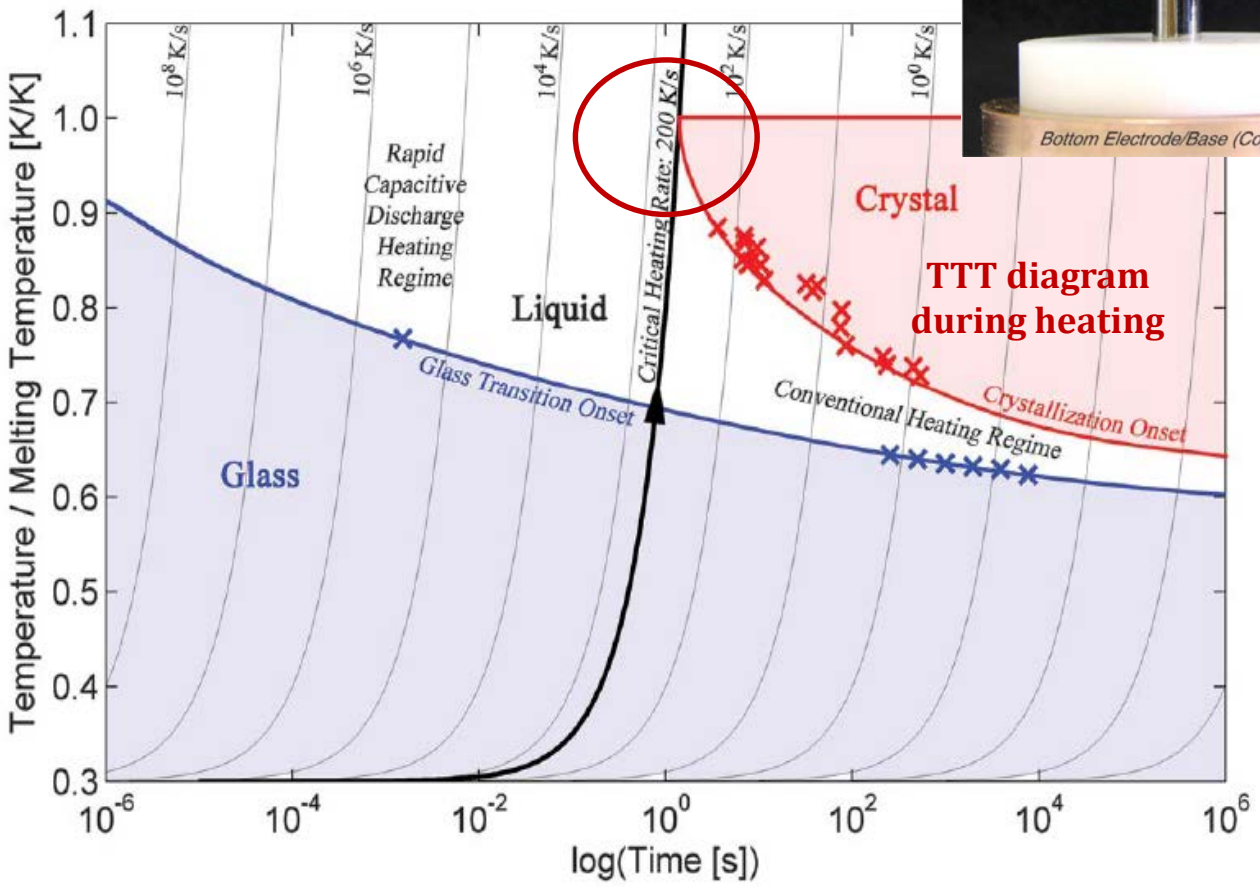

Glass transition onset temperature and crystallization onset temperature versus time for VIT 1

Time-temperature profiles during heating

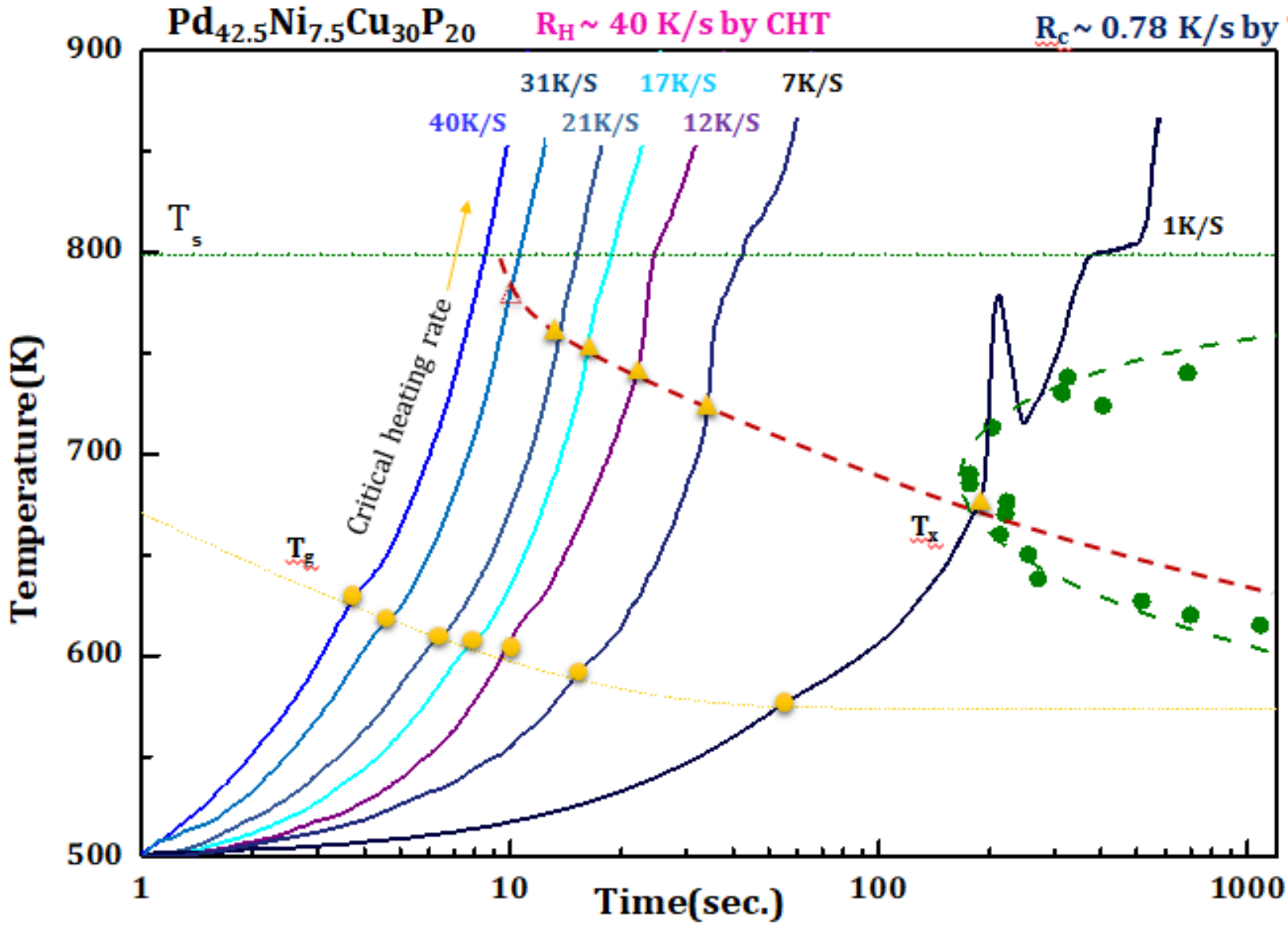

Critical heating rate (40 K/s) is 50 times faster than critical cooling rate (0.8 K/s) in PdNiCuP BMG at APS

5 *Crystallization Behavior*

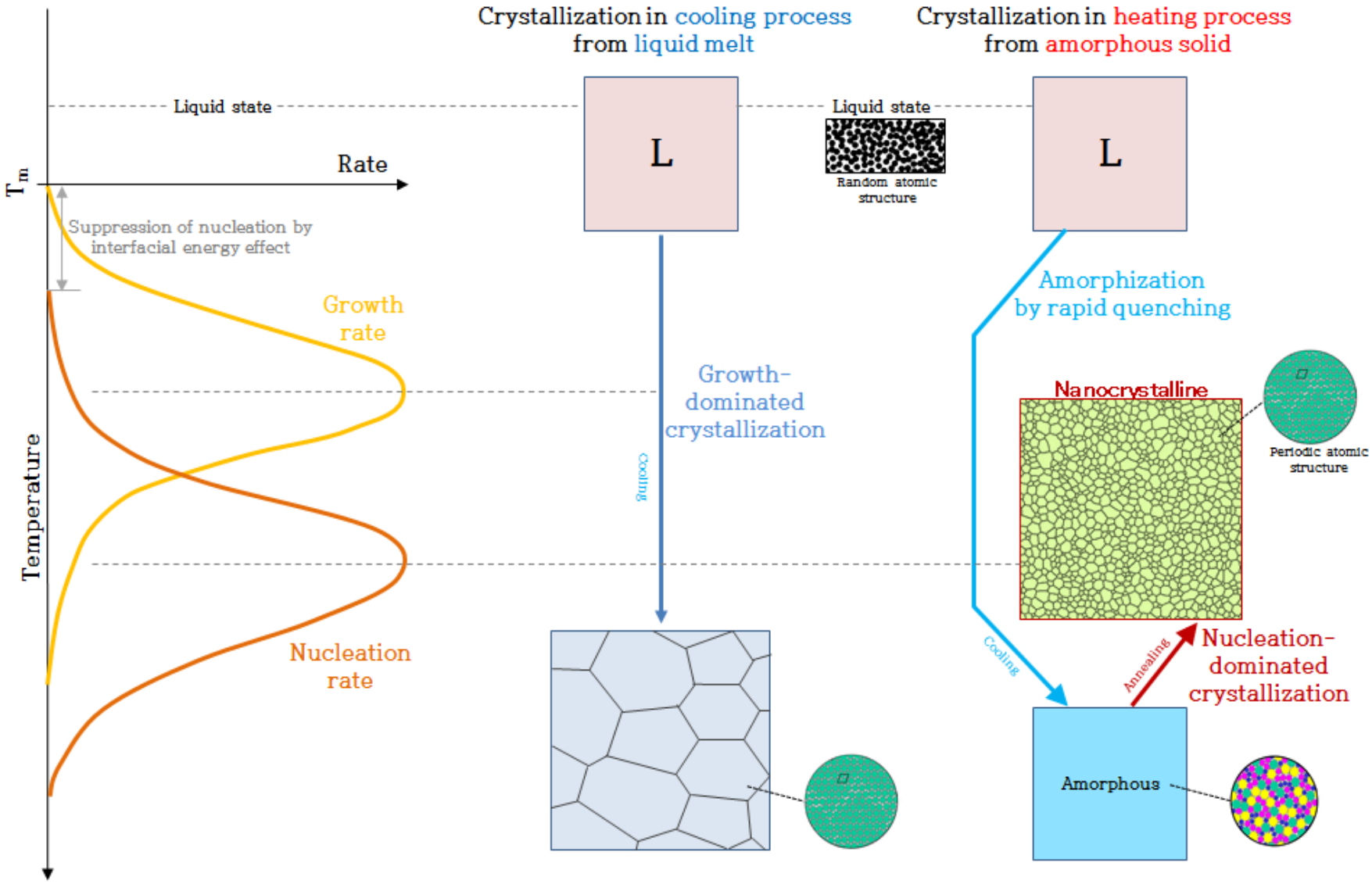

5.2.3 Structural Details

- **Amorphous vs Nanocrystalline**

1) *Microstructural observation*

XRD, (HR)TEM, *EXAFS …*

2) *Thermal analysis*

DSC (Differential Scanning Calorimetry)

: Measure heat absorbed or liberated during heating or cooling

cf) **a) *glass*** → ***nucleation & growth***

(perfect random)

b) *local clustering*: quenched-in nuclei → ***only growth***

c) *Nanocrystalline* → ***growth***

Simple idea of analytical tools

Electron
X-ray
Laser
Light
Shockwave
Mechanical

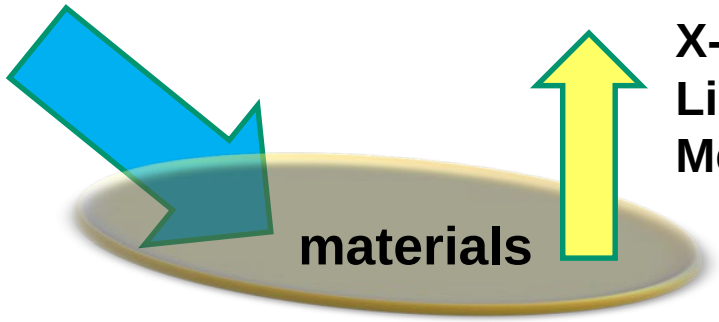

Electron
X-ray
Light
Mechanical

Analytical tool	Abbreviation	Source	Signal	Main Analysis
X-ray diffraction	XRD	X-ray	X-ray	Structure
Transmission Electron Microscopy Scanning Electron Microscopy	TEM SEM	Electron	Electron, Photon (X-ray, Light)	Structure/ Chemistry
X-ray Photoelectron Spectroscopy	XPS	X-ray	Electron	Surface chemistry/ bonding
Auger Electron Spectroscopy	AES	Electron	Electron	Surface chemistry
Energy Dispersive Spectroscopy Wavelength Dispersive Spectroscopy	EDS WDS	Electron	X-ray	Chemistry
Electron BackScattered Diffraction	EBSD	Electron	Electron	Structure/ chemistry

< X-ray diffraction >

Crystallization after annealing

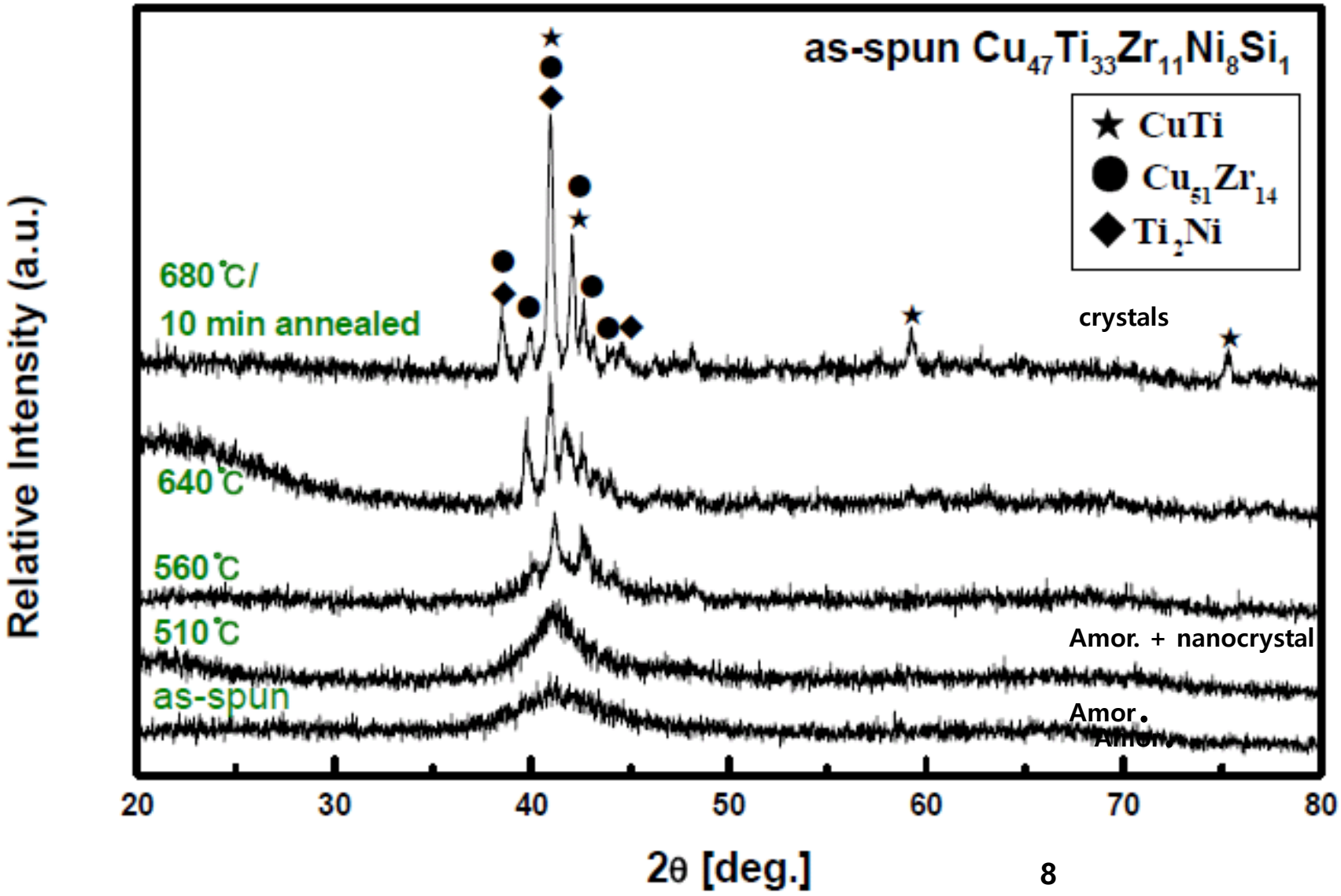

Electron Diffraction Pattern--Spot to Ring

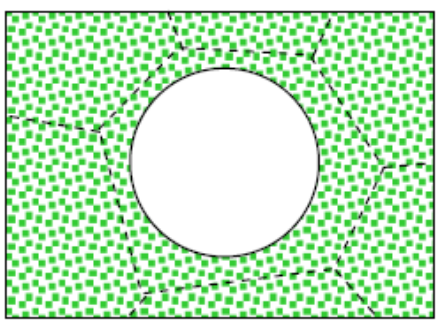

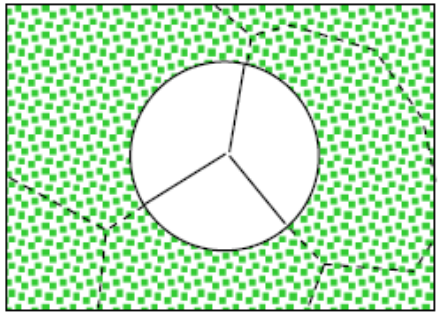

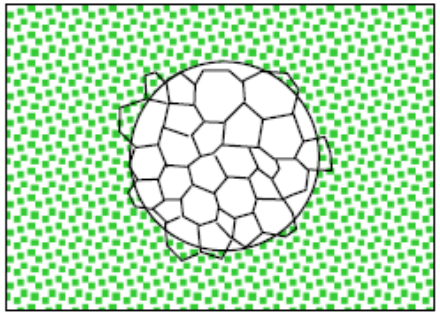

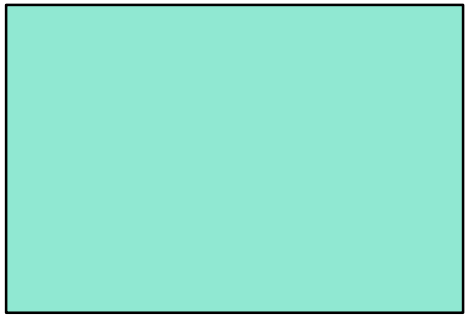

(a)

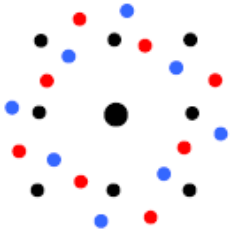

(b)

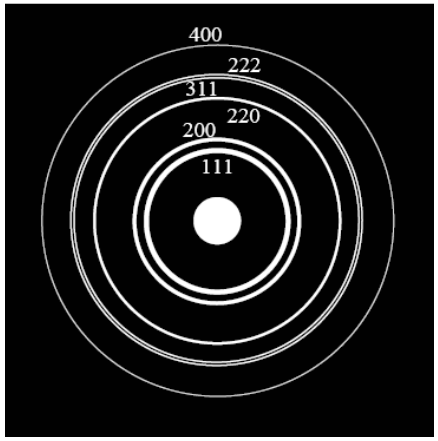

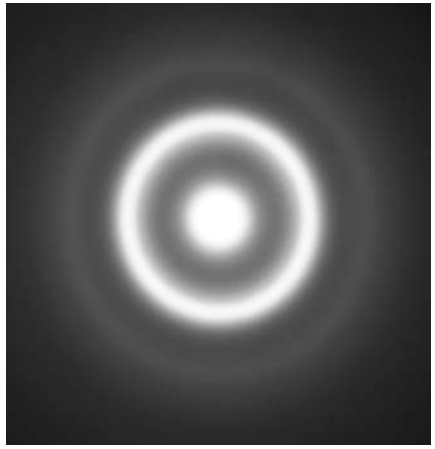

Angle range of Small angle scattering

- Length scale of small angle scattering : 1 – 1000 um

- Information on relatively large ***r*** is contained in ***I(q)*** at relatively small ***q (=4πsinθ/λ)***

- Bragg's law : ***sinθ=λ/2d***

d = few Å ***λ*** = 1 Å ***2θ*** = 20
d = 100 Å ***λ*** = 1 Å ***2θ*** = 0.6

- Sample contains a scattering length density inhomogeneity of dimension larger than 1 nm, scattering becomes observable in small angle region (0 ~ 4º)

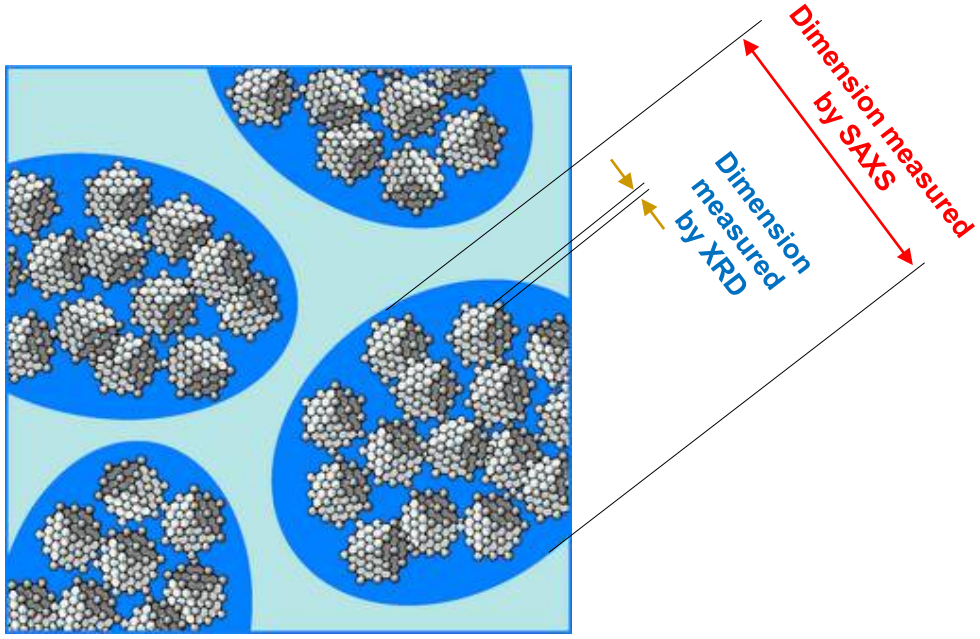

Diffraction v.s. Small angle scattering

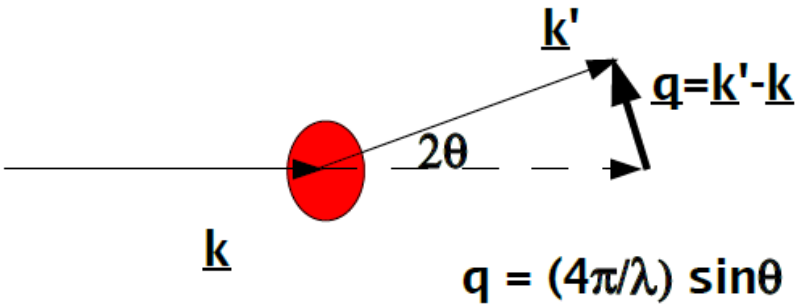

x-rays scatter from *electrons*

neutrons scatter from *nuclei* and *magnetic moments*

diffraction

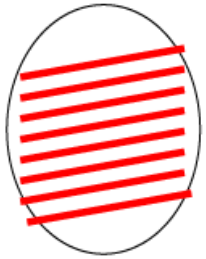

- scattering from *atomic structures*
- size of objects ~ λ
- small length scale -> large angle

small-angle scattering

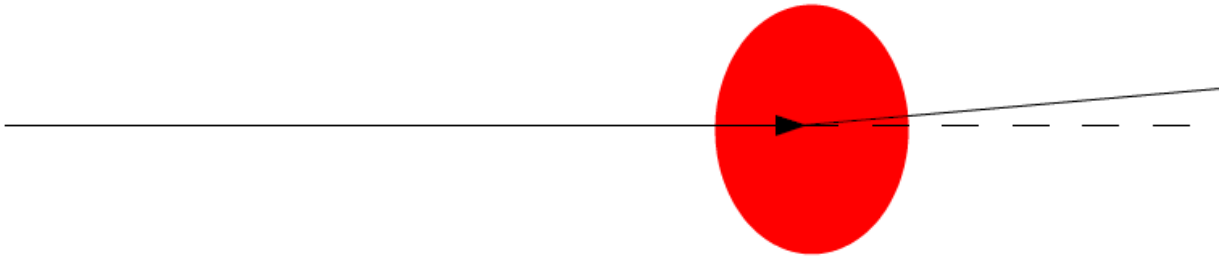

- scattering from *interfaces*
- size of objects >> λ
- large length scale -> small angle

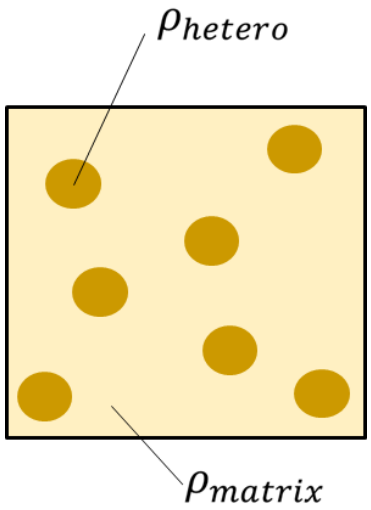

Scattering length density (of heterogeneities)

$$\rho = \frac{\sum_j^n b_j}{\bar{V}}$$

$$\Delta\rho = \rho_{hetero} - \rho_{matrix}$$

$$\bar{V} = \frac{M_w}{N_A \cdot \rho_{mass}}$$

Intensity in small angle scattering

$$I(q) = \Delta\rho^2 d_N \int_0^R N(r)[V(r)F(q,r)]^2 dr$$

d_N : number density factor
N(r) : normalized size distribution
V(r) : Volume
F(q,r) : Form factor of particles

Common factors in both SANS and SAXS

$\Delta\rho = \rho_{hetero} - \rho_{matri}$

Coherent and Incoherent Scattering

items	X-ray	neutron
source	collision of electrons with target metals(Cu, Mo, W…) acceleration of charged particles	nuclear reactor spallation neutron source (accelerator)
scattered by	electrons	atomic nuclei, unpaired spins
interaction	EM(electromagnetic)	Nuclear(strong int.) EM
scattering amplitude	linearly depend on Z	nearly indep. on Z
sample amount	μg ~ mg	~g
meas. time	$10^{1\sim2}$min (step scan: ~hr)	$10^{0\sim2}$ hr
hard to see	relatively light elements (H, Li, B, C, O …)	highly abs. nuclei (Gd, Sm, Eu, Cd, B…)

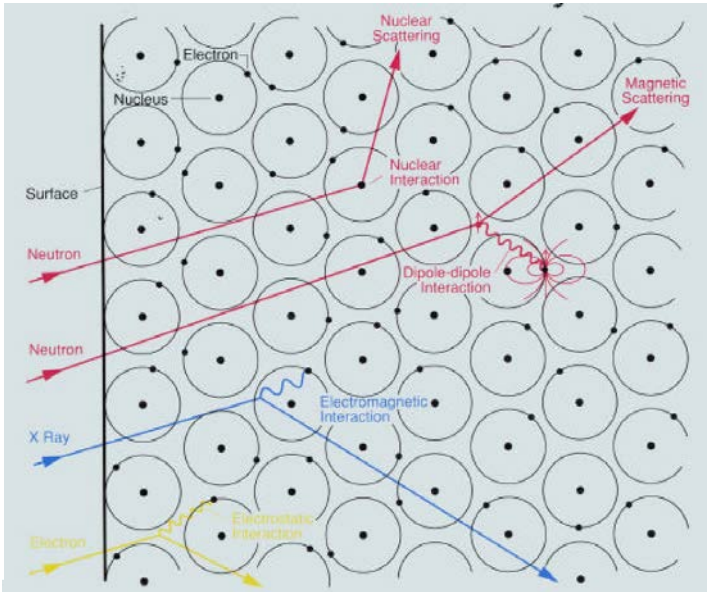

From the Roger Pynn's lecture

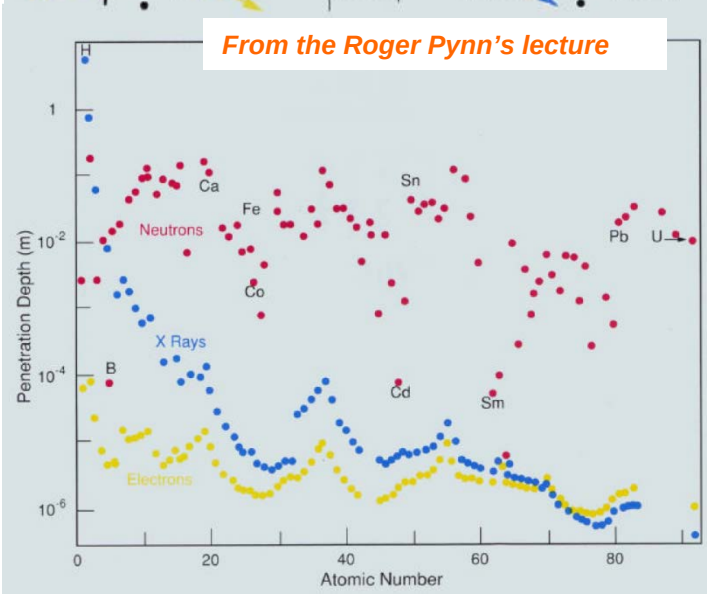

Characterizing the structure - radial distribution function,
also called pair distribution function

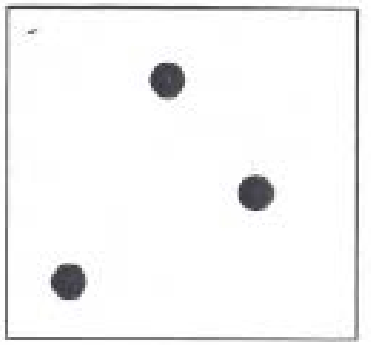

(a)

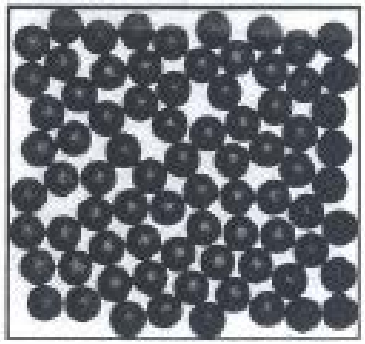

(b)

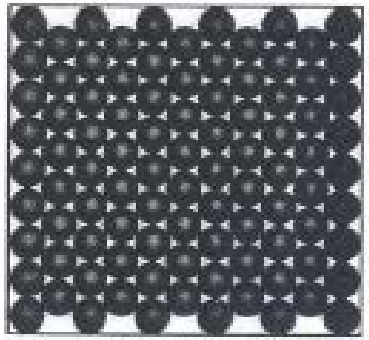

(c)

Figure 2.4 Hard-sphere model of (*a*) gas, (*b*) liquid/glass, and (*c*) crystalline solid.

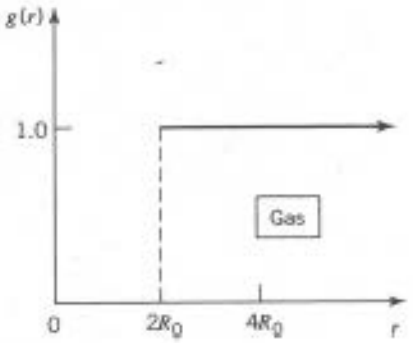

(a)

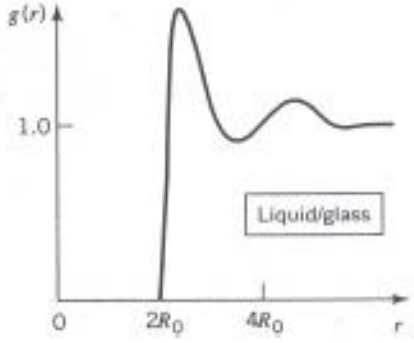

(b)

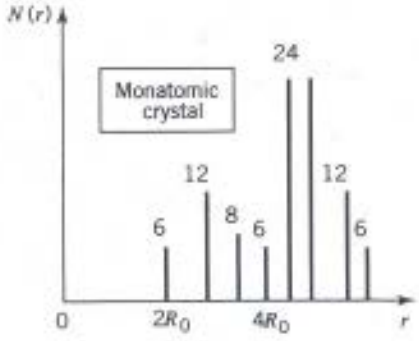

(c)

Figure 2.5 Pair-distribution functions for (*a*) a gas and (*b*) liquid or glass. (*c*) The radial dependence of the number of neighbors $N(r)$ for a primitive cubic crystal with one atom per lattice site.

Gas, amorphous/liquid and crystal structures have very different radial distribution function

Radial distribution function - definition

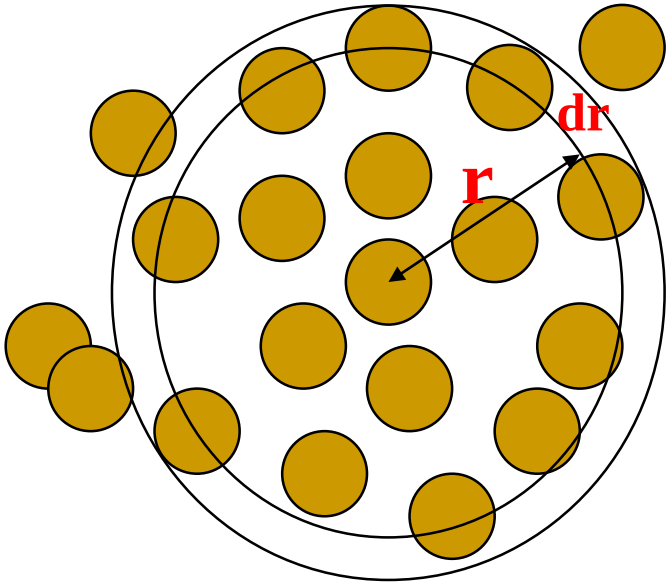

$$g(r) = \frac{1}{\langle \rho \rangle} \frac{dn(r, r+dr)}{dv(r, r+dr)}$$

1. **Carve a shell of size r and r + dr around a center of an atom.**

   The volume of the shell is

   $dv = 4\pi r^2 dr$

1. **Count number of atoms with centers within the shell (*dn*)**
2. **Average over all atoms in the system**
3. **Divide by the average atomic density <ρ>**

RDF: count the neighbors

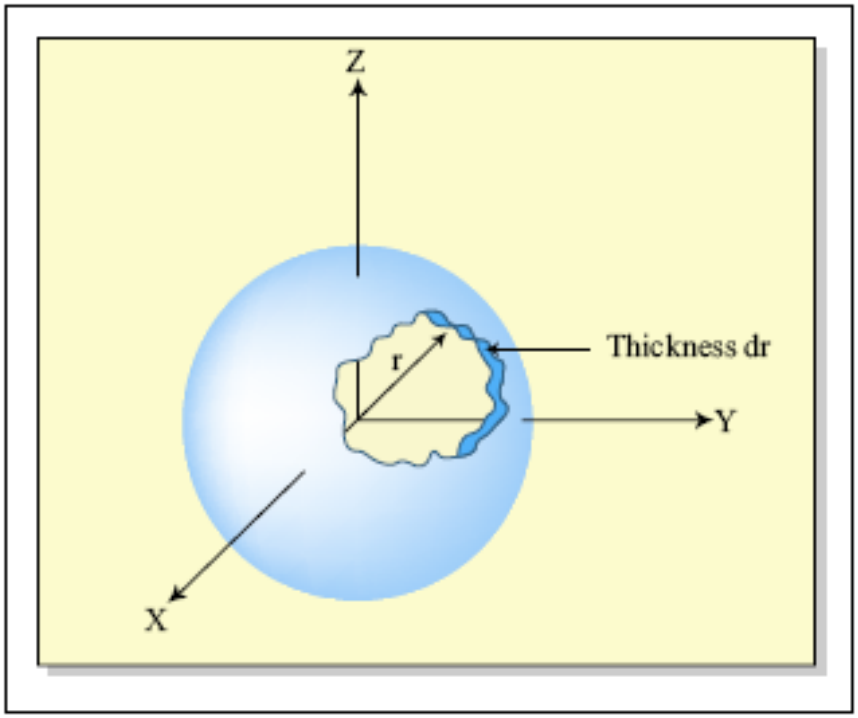

Figure by MIT OCW.

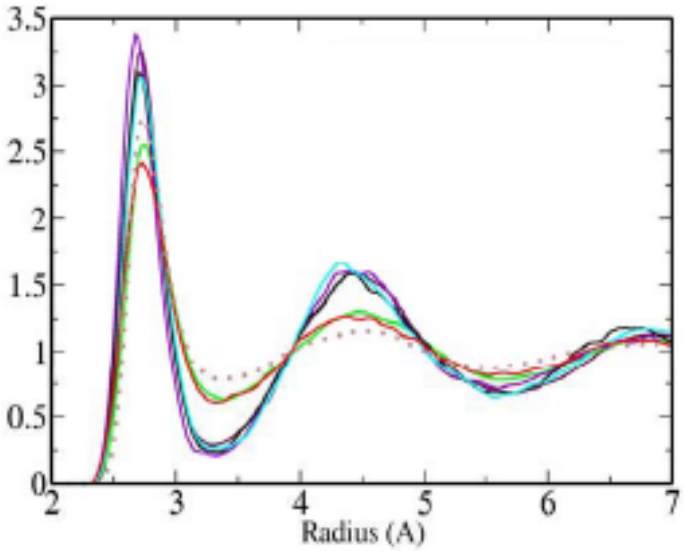

Properties of the radial distribution function

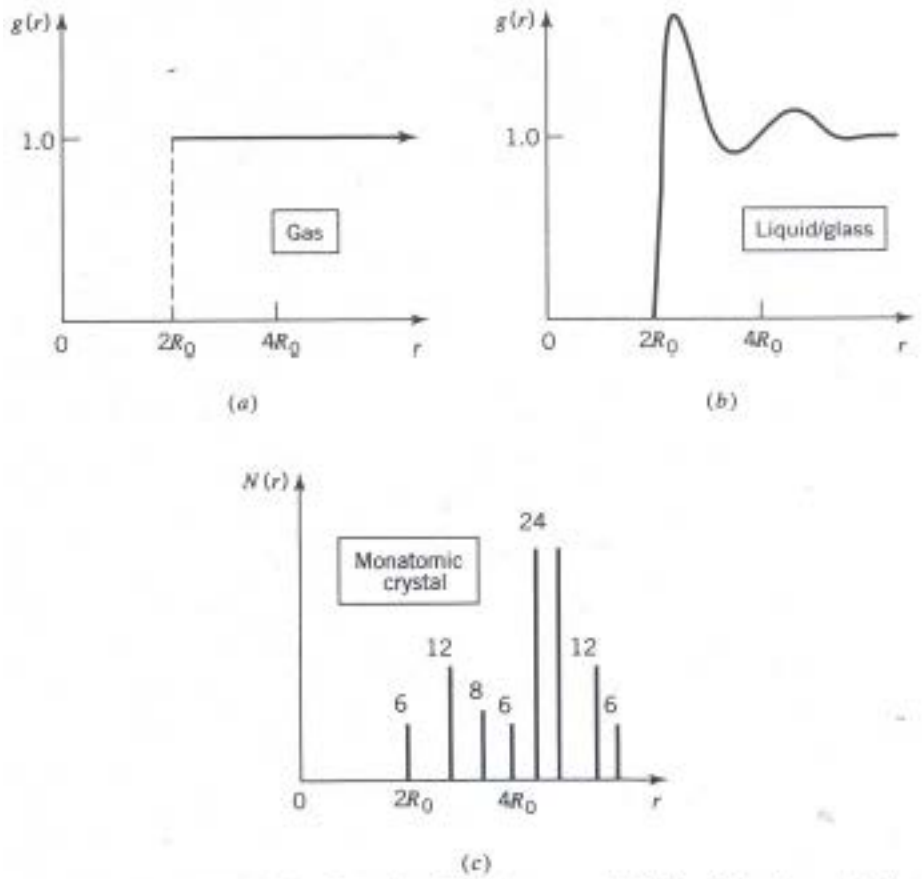

Figure 2.5 Pair-distribution functions for (*a*) a gas and (*b*) liquid or glass. (*c*) The radial dependence of the number of neighbors $N(r)$ for a primitive cubic crystal with one atom per lattice site.

For gases, liquids and amorphous solids g(r) becomes unity for large enough r.

Features in g(r) for liquids and amorphous solids are due to packing (exclude volume) and possibly bonding characteristics.

The distance over which g(r) becomes unity is called the correlation distance which is a measure of the extent of so-called short range order (SRO)

The first peak corresponds to an average nearest neighbor distance.

Radial Distribution Function - Crystal and Liquid

$$Q(r) = g(r) - 1 \sim \frac{1}{r}\sin(r/d + \varphi)\exp(r/\lambda)$$

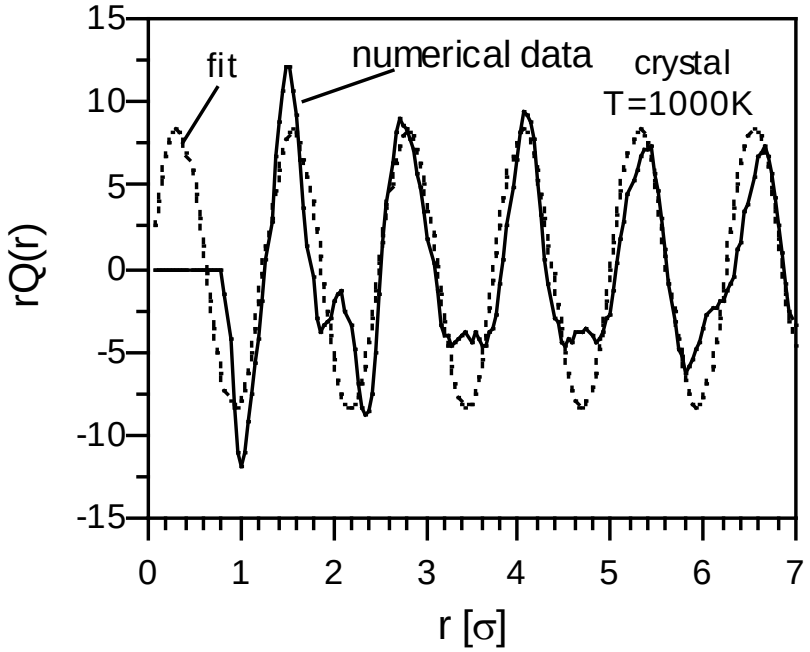

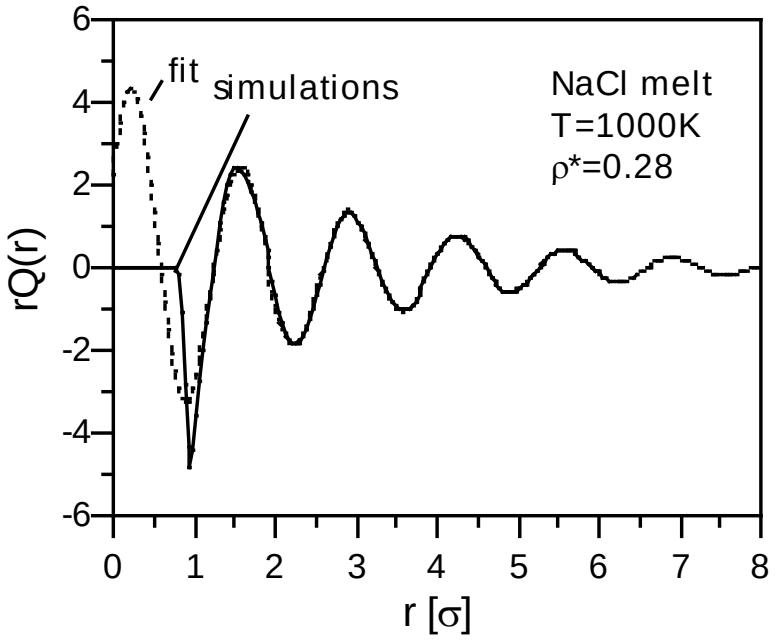

- **Liquid/amorphous g(r), for large r exhibit oscillatory exponential decay.**
- **Crystal g(r) does not exhibit an exponential decay ($\lambda \to \infty$).**

Radial distribution functions and the structure factor

- **The structure factor, S(k)**, which can be measured experimentally (e.g. by X-rays) is given by the **Fourier transform of the radial distribution function** and vice versa.

$$S(k) = 1 + \frac{4\pi\langle\rho\rangle}{k}\int_0^\infty r[g(r)-1]\sin(kr)dr$$

Radial distribution functions can be obtained from experiment and compared with that from the structural model.

→ More detailed structural characterization - Voronoi Polyhedra

Your Assignment : study and summary for Voronoi Polyhedra and submit as a ppt file (under 5 pages)

5.2 Methodology

5.2.1 Transformation Temperatures

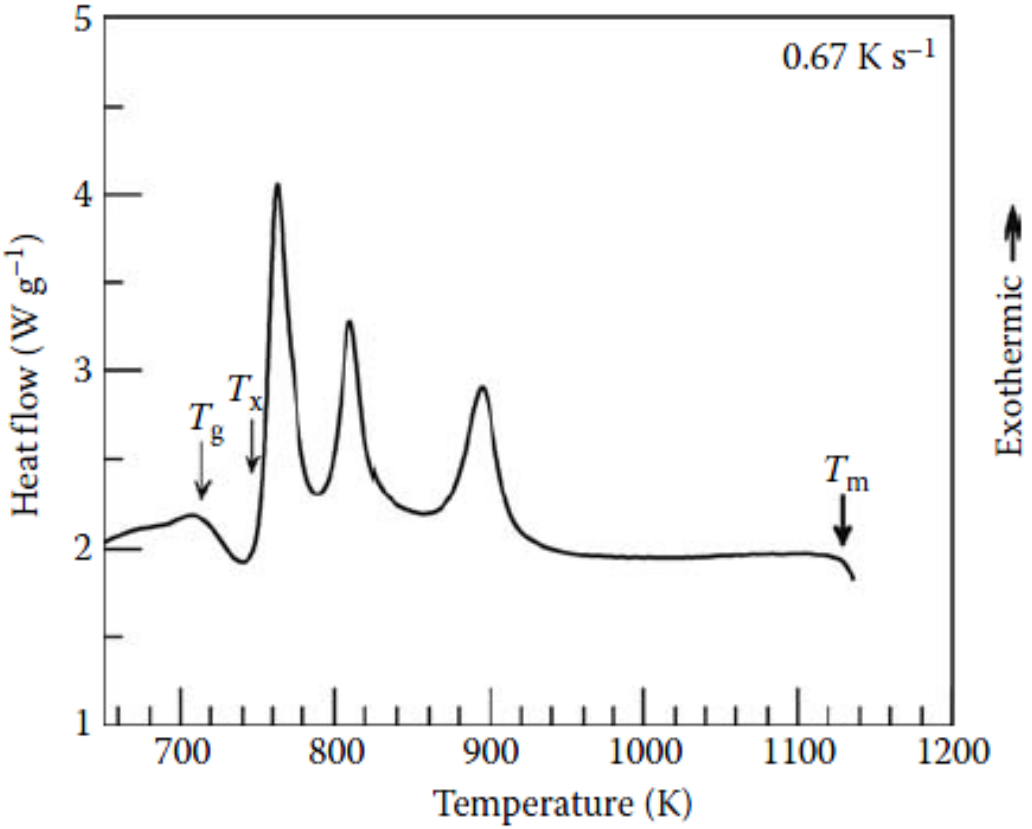

FIGURE 5.1
Schematic of a typical differential scanning calorimeter (DSC) curve obtained on heating a BMG alloy from room temperature to high temperatures at a constant heating rate of 40 K min^{-1}. Note that the curve displays three important temperatures—the glass transition temperature, T_g, the crystallization temperature, T_x, and the melting temperature, T_m. In some cases, there may be more than one crystallization temperature, depending upon the number of stages in which the glass or the supercooled liquid transforms into the crystalline phase(s).

Variation of T_g depending on alloy compositions → Broken Bonds

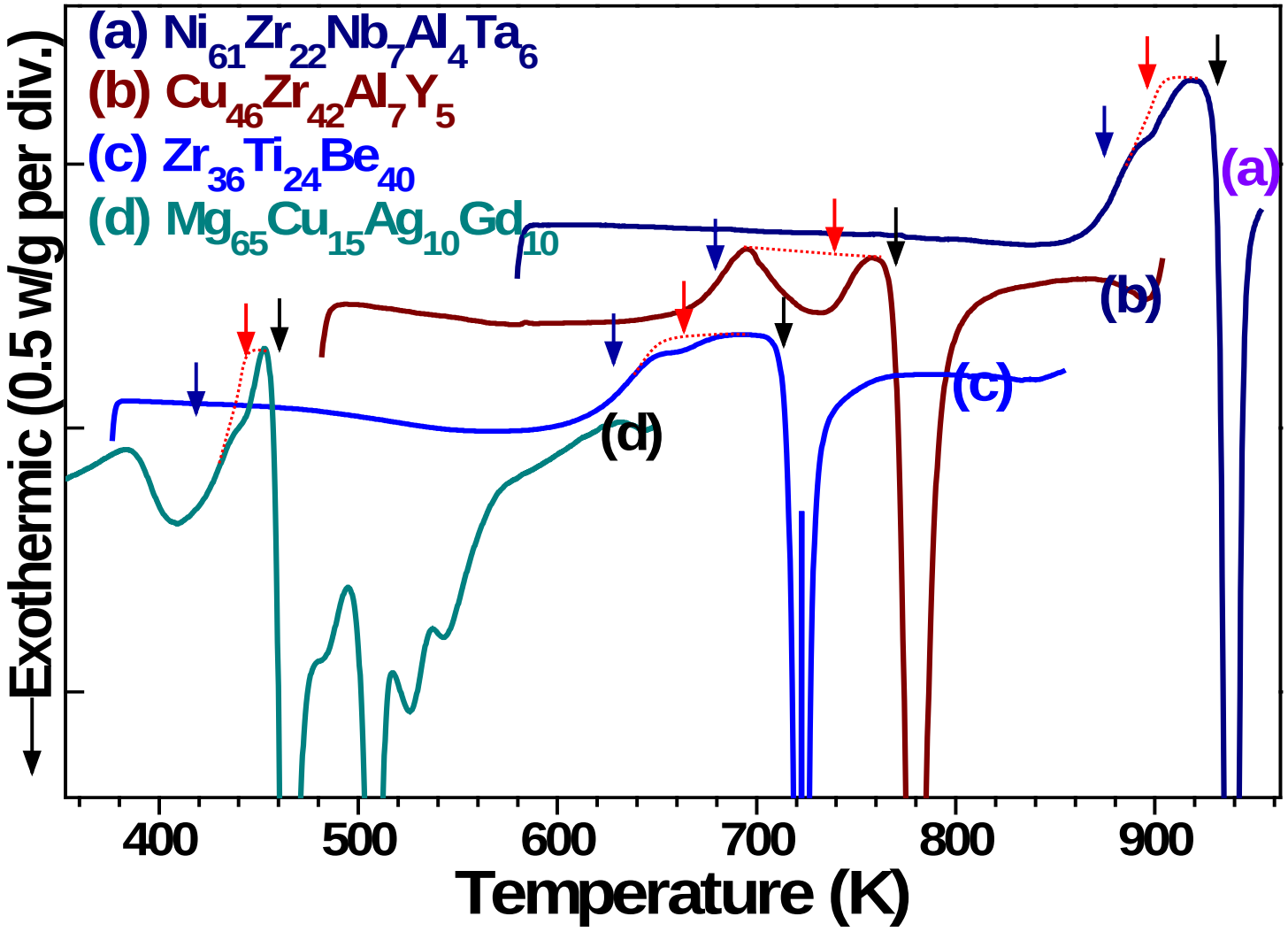

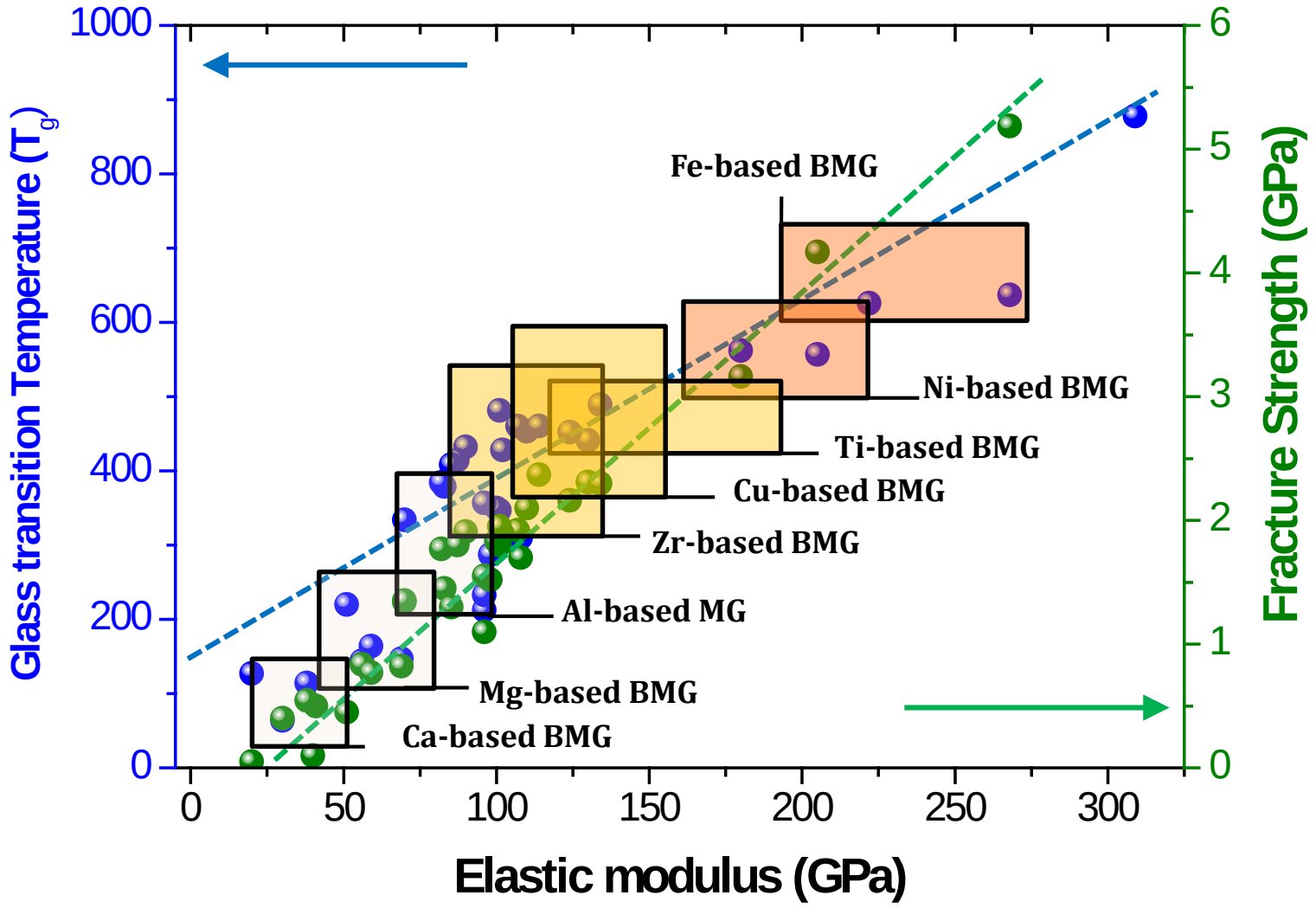
Glass transition Temperature (T_g)
Fracture Strength (GPa)
Elastic modulus (GPa)
1000
800
600
400
200
0
6
5
4
3
2
1
0
0
50
100
150
200
250
300
Fe-based BMG
Ni-based BMG
Ti-based BMG
Cu-based BMG
Zr-based BMG
Al-based MG
Mg-based BMG
Ca-based BMG

→ Almost all of the BMGs exhibit T_g. But, there are a few exceptions to this. For example, Nd-Fe-Al and Pr-Fe-Al glassy alloys did not exhibit any T_g, even though $D_{max} > 10$ mm.

TABLE 5.1

Transformation Temperatures Determined for Some Typical BMG and Melt-Spun Glassy Alloys

Composition	Glass-Forming Technique		T_g (K)	T_x (K)	ΔT_x ($=T_x - T_g$) (K)	Heating Rate (K s^{-1})[a]
$Au_{55}Cu_{25}Si_{20}$	Cu-mold casting	low	348	383	35	0.33
$Ca_{66.4}Al_{33.6}$	Cu-mold casting		528	540	12	0.33
$Ca_{60}Al_{30}Ag_{10}$	Cu-mold casting		483	531	48	0.33
$Ca_{58}Al_{32}Mg_{10}$	Cu-mold casting		513	539	26	0.33
$Ca_{65}Mg_{15}Zn_{20}$	Cone-shaped Cu-mold casting		374	412	38	0.67
$Ce_{60}Al_{10}Ni_{10}Cu_{20}$	Suction casting		374	441	67	0.167
$Co_{43}Fe_{20}Ta_{5.5}B_{31.5}$	Cu-mold casting	high	910	982	72	0.67
$Cu_{50}Zr_{50}$	Cu-mold casting		675	732	57	0.67
$Cu_{50}Zr_{50}$	Melt spinning		686	744	58	0.67
$Cu_{60}Zr_{30}Ti_{10}$	Cu-mold casting (2.5 mm dia rod)		714	758	44	0.67
$Cu_{60}Zr_{30}Ti_{10}$	Melt spinning		711	754	43	0.67
$Cu_{46}Zr_{42}Al_7Y_5$	Injection casting into Cu-mold (10 mm dia rod)		672	772	100	0.33
$Fe_{64}Mo_{14}C_{15}B_7$	Injection casting into Cu-mold (2.5 mm dia rod)		793	843	50	0.33
$Hf_{52.5}Cu_{17.9}Ni_{14.6}Al_{10}Ti_5$	Suction casting		767	820	53	0.167
$La_{55}Al_{25}Ni_{10}Cu_{10}$	High-pressure die casting (9 mm dia rod)		460	527	67	0.67
$La_{55}Al_{25}Ni_{10}Cu_{10}$	Melt spinning		460	550	90	0.67
$Mg_{65}Cu_{7.5}Ni_{7.5}Zn_5Ag_5Y_{10}$	Melt spinning		430	459	29	0.67
$Ni_{60.25}Nb_{39.75}$	Injection casting into Cu-mold (1 mm dia rod)		891	923	32	0.33
$Ni_{62}Nb_{33}Zr_5$	Injection molding (3 mm dia rod)		877	917	40	0.33
$Pd_{79}Ag_{4.5}Si_{16.5}$	Splat cooling		640	672	32	0.33
$Pd_{78}Ag_{5.5}Si_{16.5}$	Dropping a molten droplet onto metal substrate		642	683	41	0.33
$Pd_{80}Au_{3.5}Si_{16.5}$	Splat cooling		644	675	31	0.33
$Pd_{78}Au_4Si_{18}$	Roller quenching		656	696	40	0.67

TABLE 5.1

Transformation Temperatures Determined for Some Typical BMG and Melt-Spun Glassy Alloys

Composition	Glass-Forming Technique	T_g (K)	T_x (K)	ΔT_x ($=T_x - T_g$) (K)	Heating Rate (K s^{-1})[a]
$Pd_{43}Cu_{27}Ni_{10}P_{20}$ (fluxed)	Water quenching	585	716	largest 131	0.67
$Pd_{43}Cu_{27}Ni_{10}P_{20}$ (foam)	Water quenching	577	667	90	0.33
$Pd_{40}Cu_{30}Ni_{10}P_{20}$ (unfluxed)	Melt spinning	572	663	91	0.33
$Pd_{40}Cu_{30}Ni_{10}P_{20}$ (fluxed)	Melt spinning	572	670	98	0.33
$Pd_{77.5}Cu_6Si_{16.5}$	Dropping a molten droplet onto metal substrate	646	686	40	0.33
$Pd_{40}Ni_{40}P_{20}$	Centrifugal spinning	583	650	67	0.33
$Pd_{40}Ni_{40}P_{20}$ (fluxed)	Water quenching (7 mm dia rod)	576	678	102	0.33
$Pd_{40}Ni_{40}P_{20}$ (unfluxed)	Melt spinning	580	643	63	0.33
$Pd_{40}Ni_{40}P_{20}$ (fluxed)	Melt spinning	590	671	91	0.33
$Pd_{81}Si_{19}$ (fluxed)	Air cooling	638	696	58	0.33
$Pd_{81}Si_{19}$ (fluxed)	Melt spinning	633	675	42	0.33
$Pd_{80}Si_{20}$	Splat cooling	655	667	12	0.33
$Pr_{60}Cu_{20}Ni_{10}Al_{10}$	Suction casting	409	452	43	0.167
$Pt_{57.5}Cu_{14.7}Ni_{5.3}P_{22.5}$ (fluxed)	Water quenching (16 mm dia rod)	508	606	98	0.33
$Sm_{56}Al_{22}Ni_{22}$	Suction casting	544	582	38	0.33
$Ti_{32}Hf_{18}Ni_{35}Cu_{15}$	Planar flow casting	722	766	44	0.167
$Ti_{50}Ni_{24}Cu_{20}B_1Si_2Sn_3$	Cu-mold casting	726	800	74	0.67
$Ti_{40}Zr_{25}Ni_2Cu_{13}Be_{20}$	Cu-mold casting	599	644	45	0.33
$Y_{36}Sc_{20}Al_{24}Co_{20}$	—	645	760	115	0.67
$Zr_{65}Al_{7.5}Ni_{10}Cu_{17.5}$	Water quenching (16 mm dia rod)	625	750	125	0.67
$Zr_{65}Al_{7.5}Ni_{10}Cu_{17.5}$	Melt spinning	622	749	127	0.67
$Zr_{41.2}Ti_{13.8}Cu_{12.5}Ni_{10}Be_{22.5}$	Cu-mold casting	625	705	80	0.33

[a] 0.167 K s^{-1} = 10 K min^{-1}; 0.33 K s^{-1} = 20 K min^{-1}; and 0.67 K s^{-1} = 40 K min^{-1}.

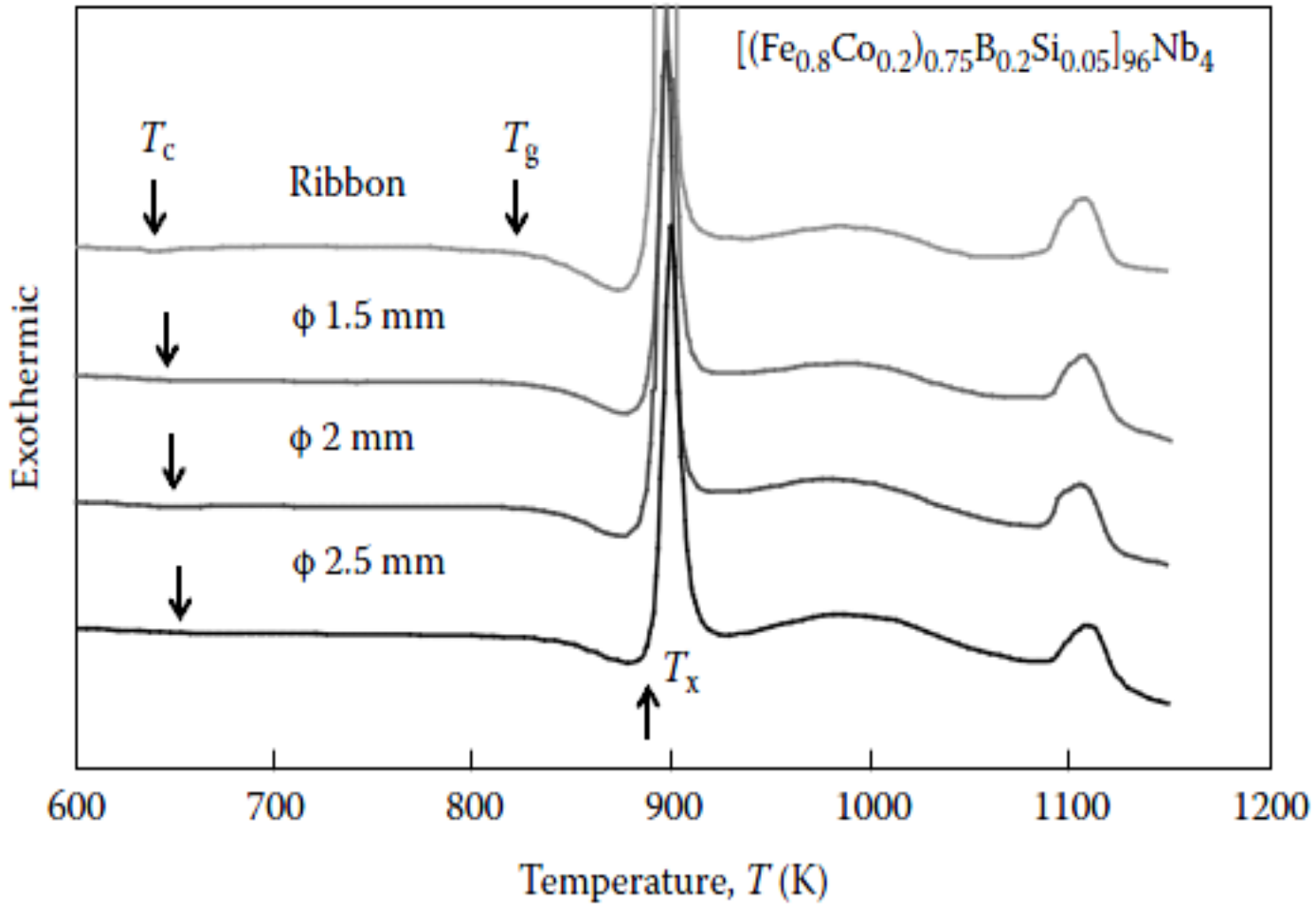

FIGURE 5.2

DSC curves of bulk glassy $[(Fe_{0.8}Co_{0.2})_{75}B_{20}Si_5]_{96}Nb_4$ alloy of different diameters (1.5, 2.0, and 2.5 mm) and melt-spun ribbon of the same composition. These curves clearly demonstrate that the transformation temperatures are identical for all the samples and that the transformation temperatures do not depend upon the diameter of the rod or the thickness of the ribbon. (Reprinted from Inoue, A. et al., *Acta Mater.*, 52, 4093, 2004. With permission.)

* Typically T_g is ~ 50-60% of the melting point.

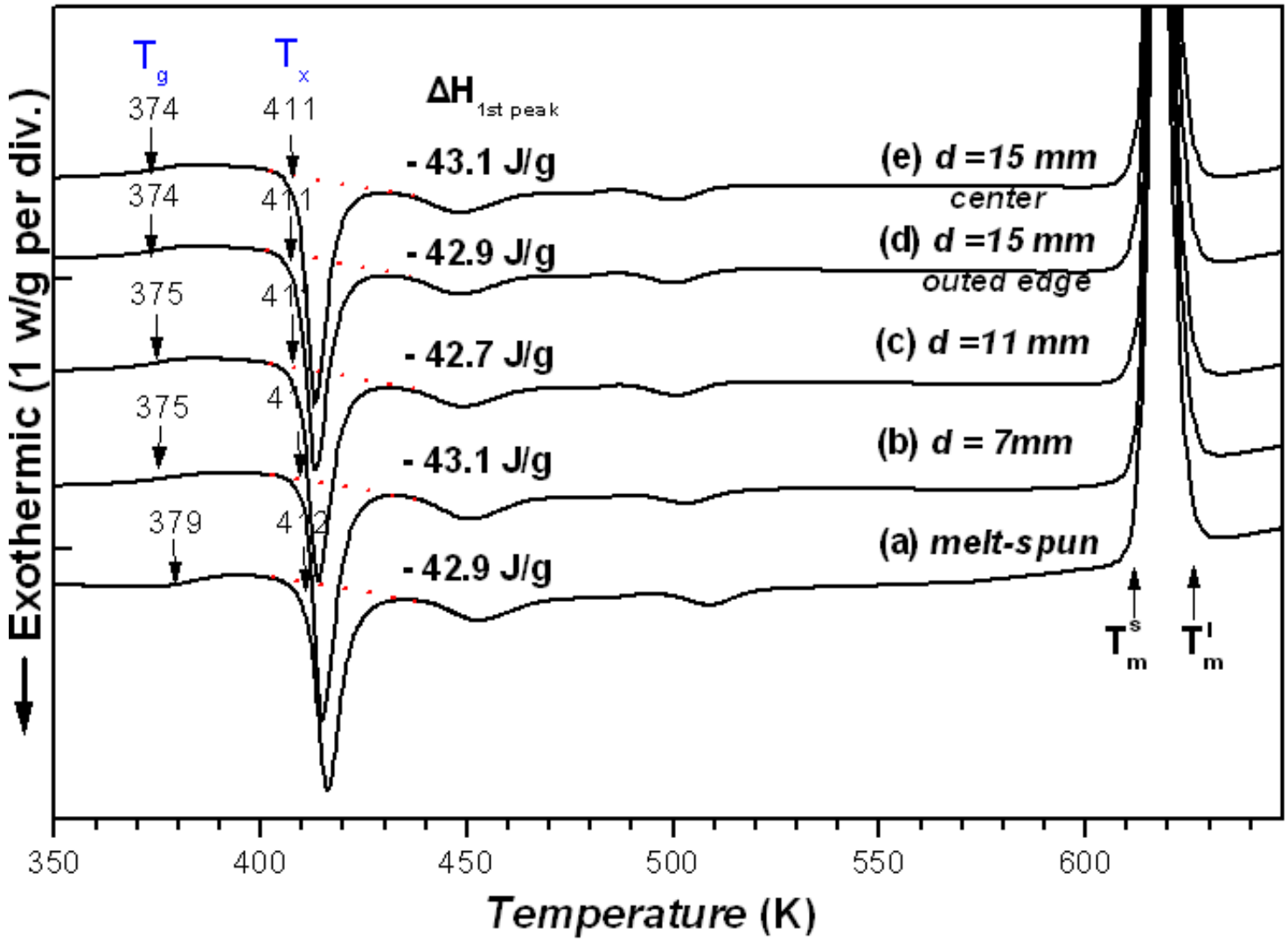

* J Mater Res, 19 (2004) 685.

The glass transition temperature T_g is a kinetic parameter and its value depends on the cooling rate at which the glass is formed (and also on the heating rate at which the glassy sample is reheated). It was also noted that T_g was lower when the glass had formed at lower cooling rates. Therefore, it would be possible to assume that the T_g for the melt-spun ribbon and BMG rod will be different. But, this is not true. The reason is that T_g, the temperature at which the glass is formed is estimated during the cooling of the molten alloy. On the other hand, T_g is usually measured experimentally during the heating of the glassy alloy that has already formed. Once the glass is heated from room temperature to higher temperatures, it is structurally relaxed and, therefore, it does not matter how the glass had initially formed. Accordingly, both types of glasses will have the same T_g and T_x temperatures, when measured at the same heating rate. That is, there is no difference between the T_g values of glasses prepared by RSP or slow solidification methods.

5.4 Differences in the Crystallization Behavior between Melt-Spun Ribbons and Bulk Metallic Glasses

(a) The melt-spun metallic glass ribbons **solidified at higher cooling rates** are farther from equilibrium than the BMGs. → **a larger decrease in density and higher energy stored** in the melt-spun ribbons → One would expect that, **due to the larger departure from equilibrium, the kinetics of crystallization in melt-spun glassy ribbons would be faster than that in BMGs. But this is not necessarily true.**

(b) Once the glass is heated to a temperature above Tg, the glass **becomes a supercooled liquid** (but still exists in the form of a solid). At this stage there is **no difference in the "structure"** between the BMG and the melt-spun metallic glass that was obtained directly by rapidly solidifying the metallic melt, **except that the extent of structural relaxation would be different in the two glasses.** → Therefore, once the BMG has been heated to **above Tg, the crystallization behavior of BMGs and melt-spun metallic glassy ribbons will be identical** (assuming that both the glasses have the same chemical composition).

5.2.2 Activation energy for crystallization

Two different methods: (a) Kissinger method, (b) Ozawa method

(a) Kissinger method

$$\ln\left(\frac{\beta}{T_p^{\,2}}\right)=\left(-\frac{Q}{RT_p}\right)+A$$

where
A is a constant
R is the universal gas constant

Thus, by plotting $\ln\left(\beta/T_p^2\right)$ against $1/T_p$, one obtains a straight line whose slope is $-Q/R$, from which the activation energy for the transformation, Q can be calculated (Figure 5.3).

- Could get the required data during continuous heating in a DSC
- Possible to evaluate the individual activation energies for the nucleation and growth stages of the transformation
- May not be useful in all studies of decomposition

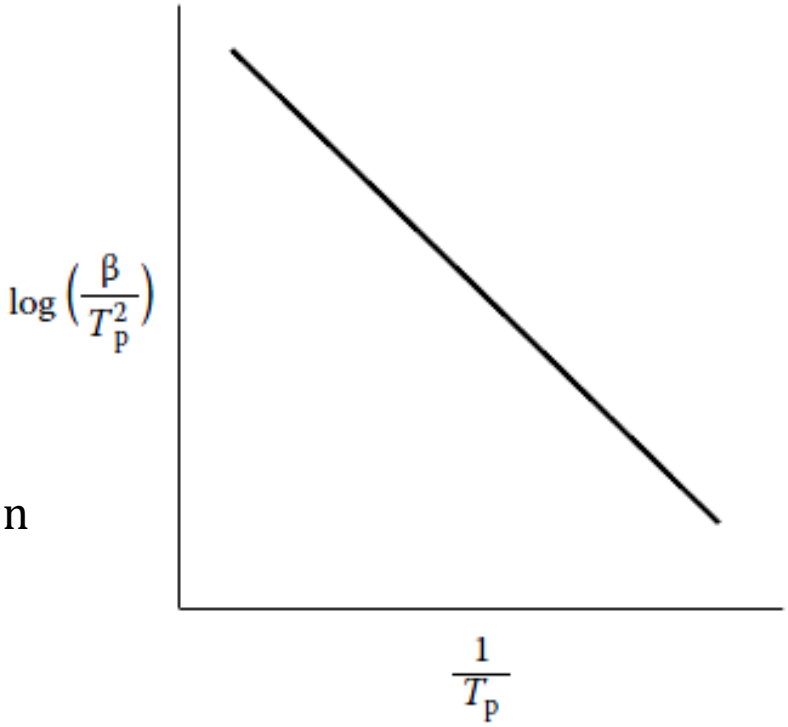

FIGURE 5.3
Kissinger plot in which $\ln(\beta/T_p^2)$ is plotted against $1/T_p$, when a straight line is obtained. The activation energy for crystallization can be calculated from the slope of this straight line.

- **Chen & Spaepen (Harvard,1988)**

a) ***glass*** → ***nucleation & growth***
(perfect random)

→ **Isothermal annealing**
: rapid heating + maintain the temp.

- ***Glass* :**

J-M-A Eq. $x = 1 - \exp(-bt^n)$ (***n: 2~4, nucleation mechanism***)

crystallized volume fraction after time t

→ ***Corresponding heat release***

$$-\frac{dH}{dt} = \Delta H(1-x)n \cdot bt^{n-1}$$

(***ΔH: total transformation enthalpy***)

Fig. 1.4 Isothermal enthalpy release rates for crystallite nucleation and growth (solid line) and crystallite grain-coarsening mechanisms (dashed line)

$$-\frac{dH}{dt} = \Delta H(1-x)n \cdot bt^{n-1}$$

Glass

: exothermic peak at non-zero time

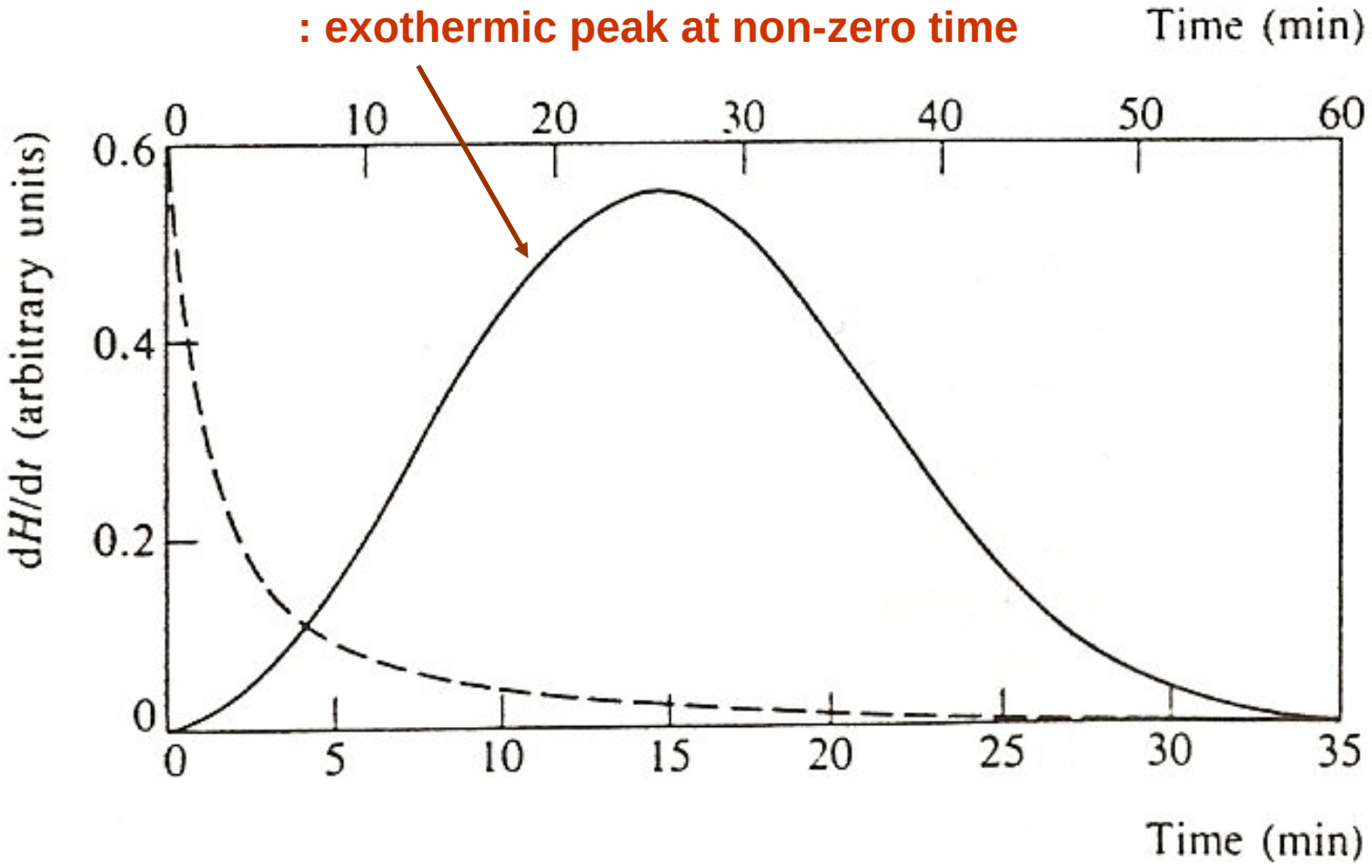

- **c) *Nanocrystalline* → *grain growth***

$$\rightarrow \quad \frac{dr}{dt} = M \cdot \frac{\gamma}{r^m}$$

(***M*: *atomic mobility*, γ : *interfacial surface tension***)

→ ***corresponding heat release***

$$-\frac{dH}{dt} = H(0) \cdot r(0) \cdot M\gamma / r^{m+2}$$

(***H(0)*: *zerotime enthalpy of a grain size of r (0)***)

→ ***Monotonically decreasing curve***

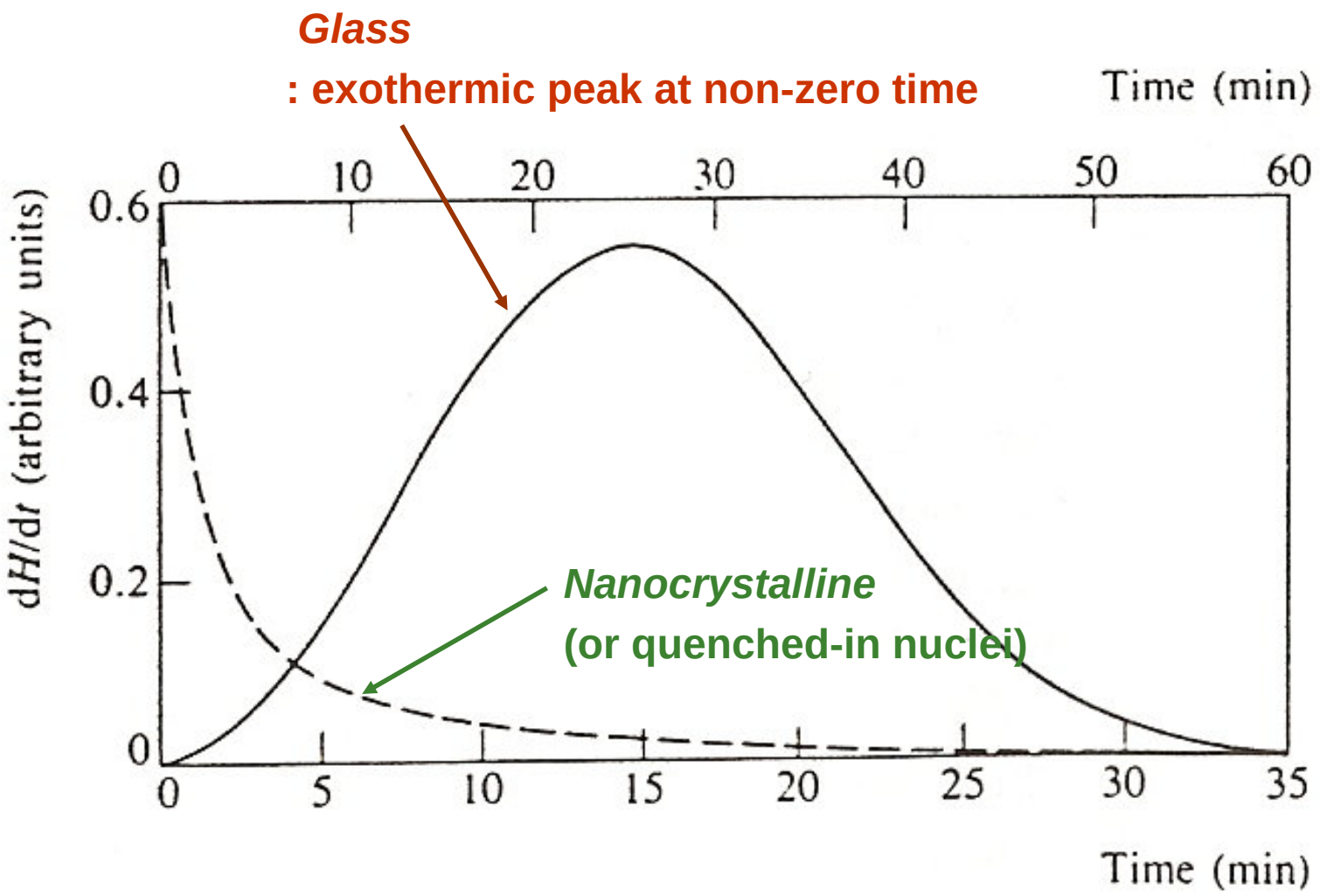

Fig. 1.4 Isothermal enthalpy release rates for crystallite nucleation and growth (solid line) and crystallite grain-coarsening mechanisms (dashed line)

Effect of quenched-in quasicrystal nuclei

2 mm rod

(a) $Zr_{63}Ti_5Nb_2Cu_{15.8}Ni_{6.3}Al_{7.9}$

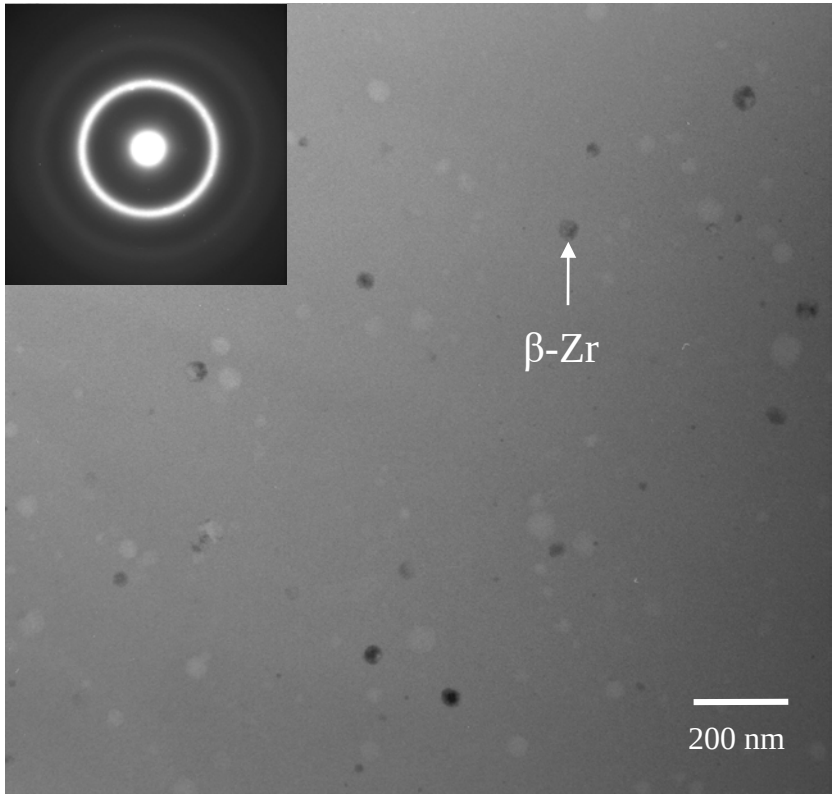

β-Zr particle (~70 nm) in amorphous matrix

(b) $Zr_{57}Ti_8Nb_{2.5}Cu_{13.9}Ni_{11.1}Al_{7.5}$

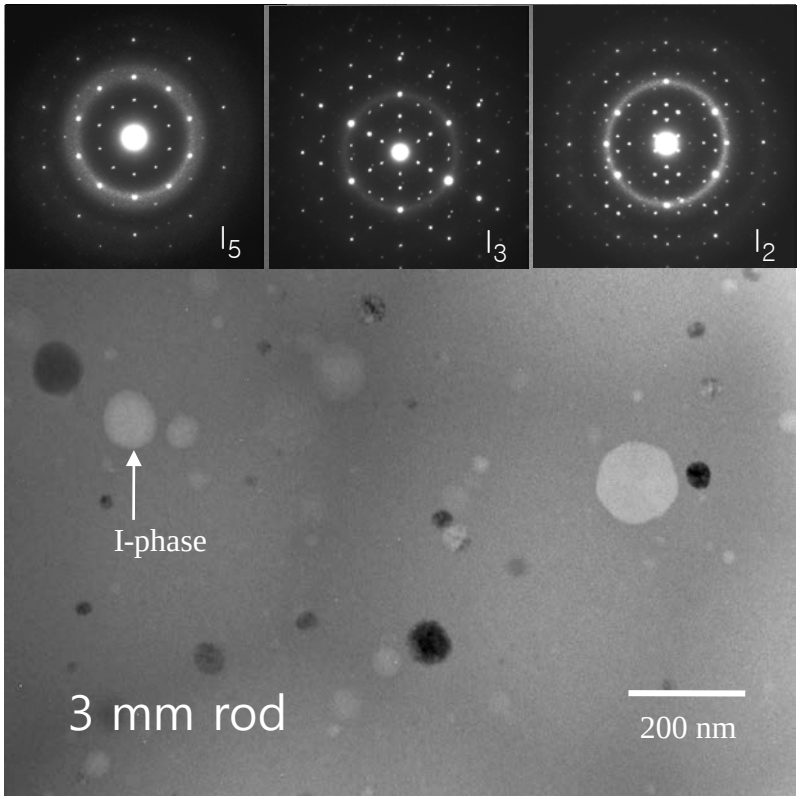

I-phase particle in amorphous matrix

Before deformation

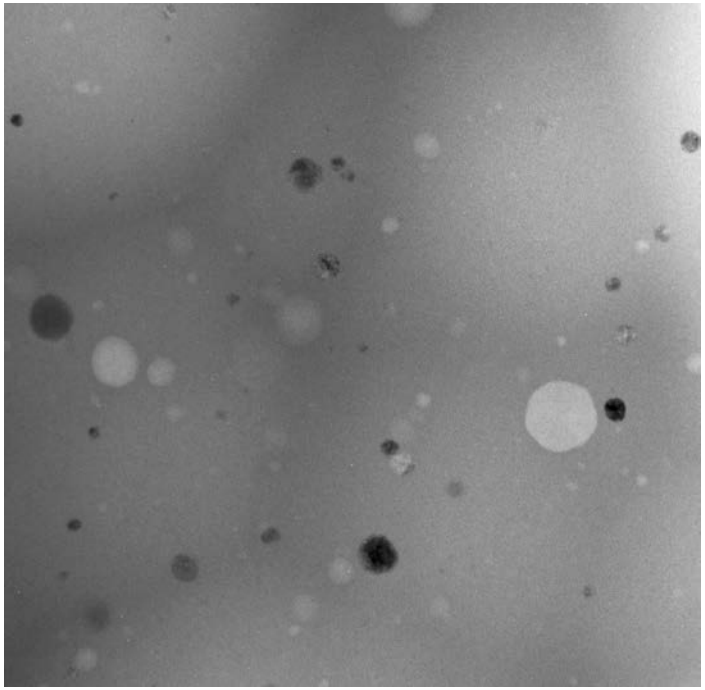

After deformation

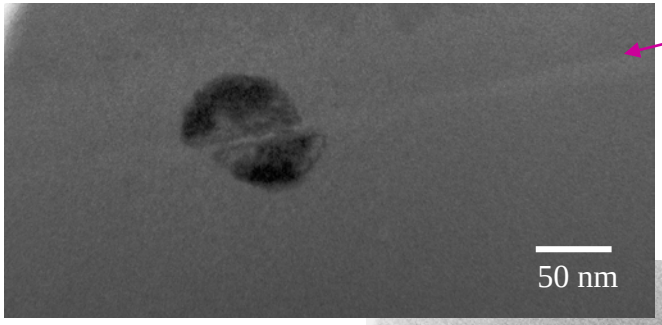

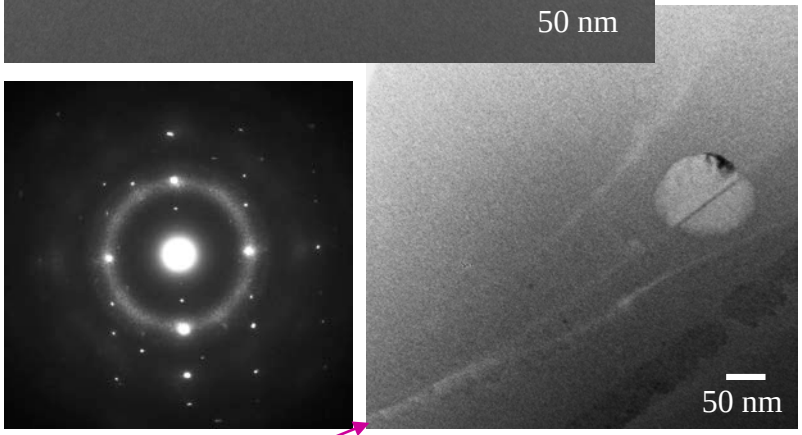

shear band

- No distribution of icosahedral particle to blocking the propagation of shear band.
- No enhancement of plasticity in MGMC with icosahedral particle

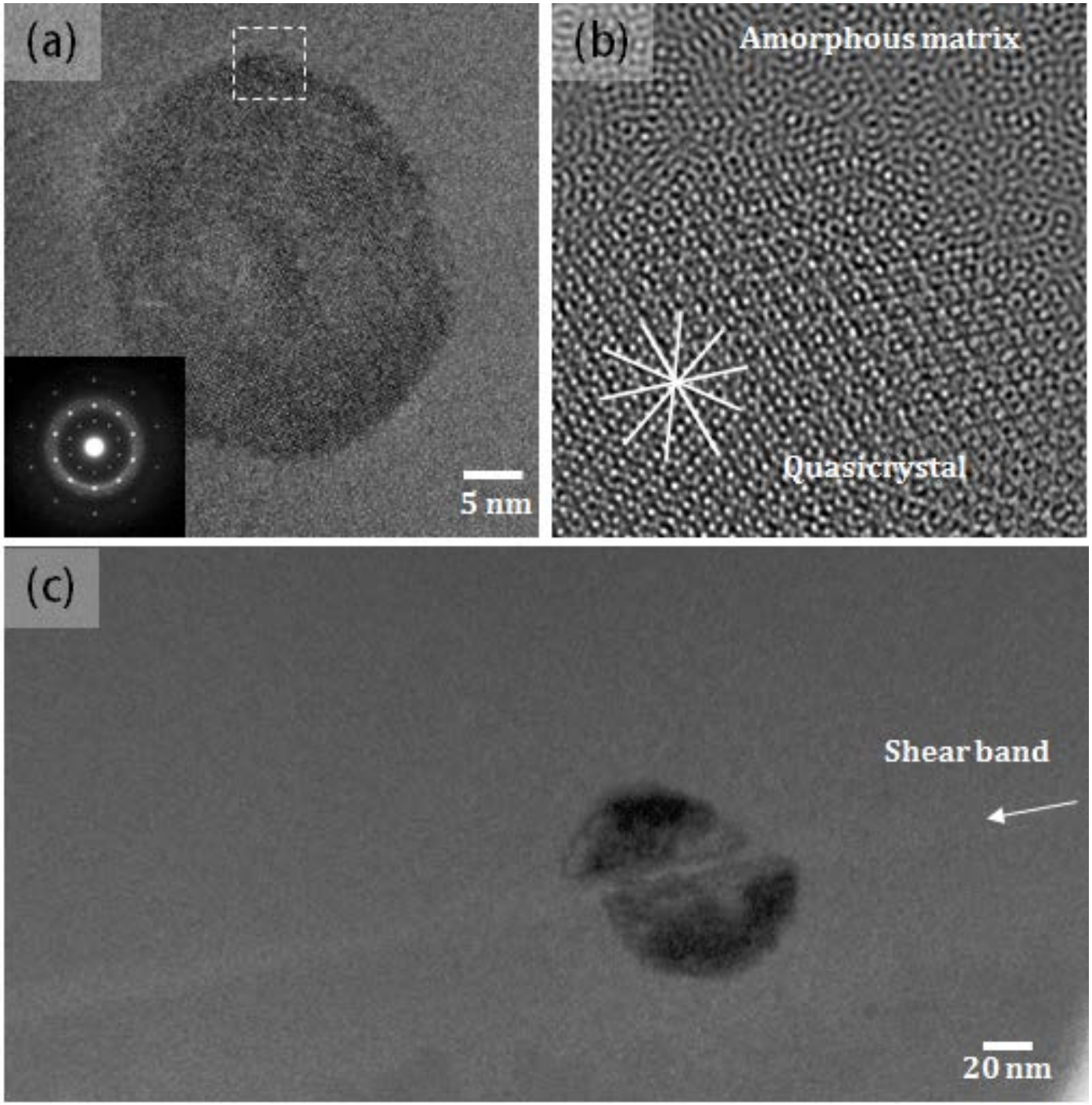
(a)
5 nm
(b)
Amorphous matrix
Quasicrystal
(c)
Shear band
20 nm

- Compression test

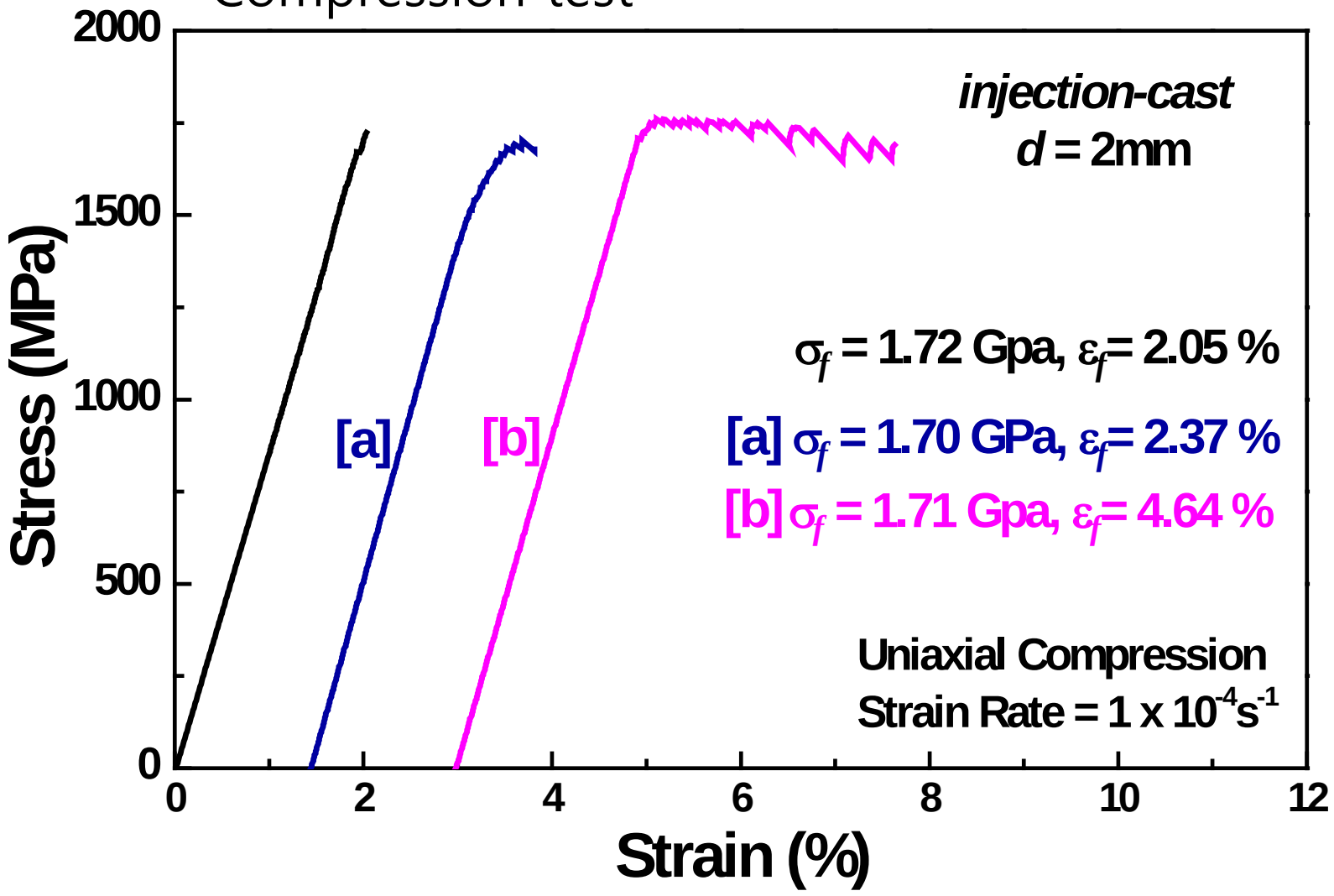

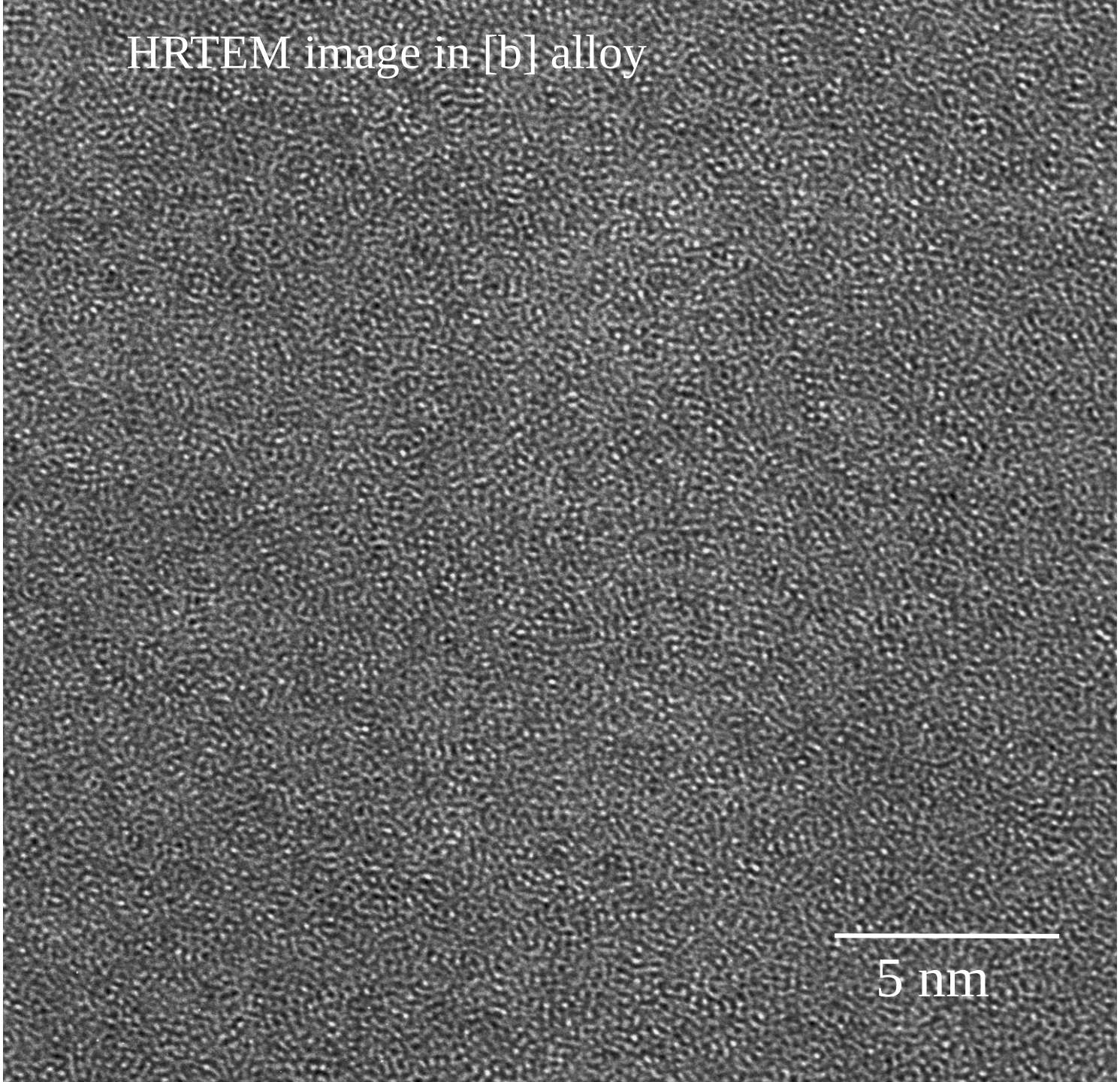
HRTEM image in [b] alloy
5 nm

- Activation E : driving force for nucleation

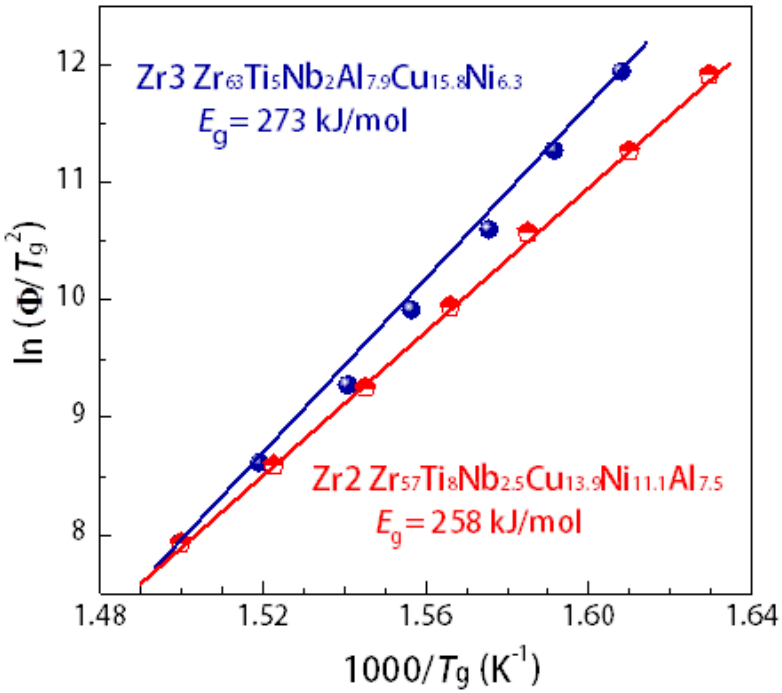

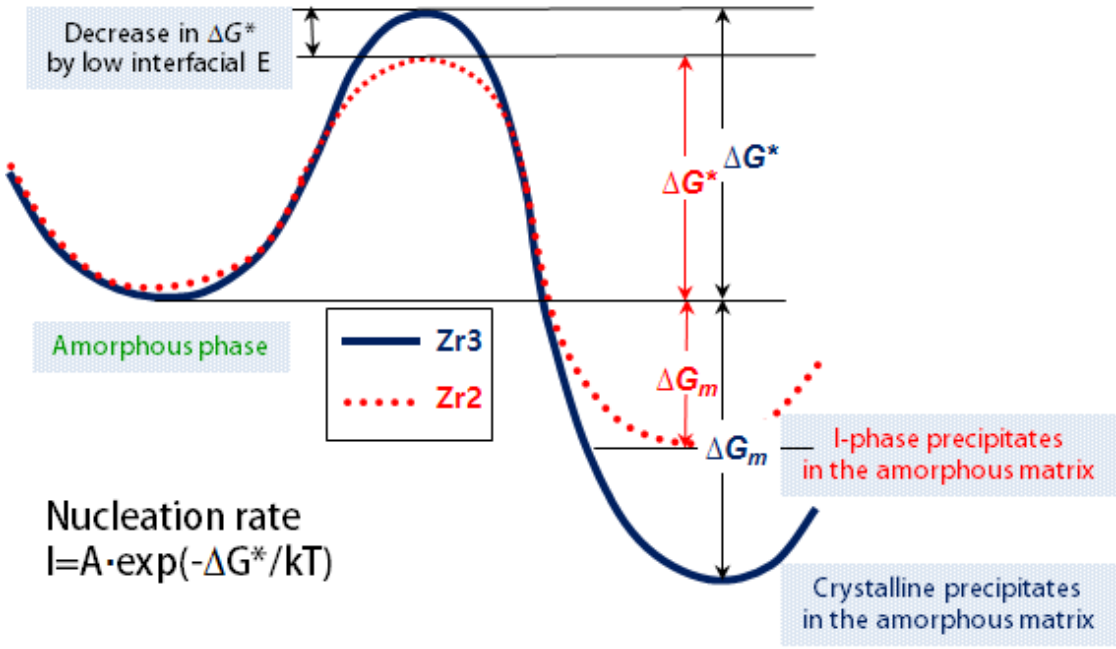

Kissinger's equation

$$\ln(\Phi / T_g^2) = -Q / RT_g + const.$$

Effect of quenched-in quasicrystal nuclei

- Isotherm in DSC

Isothermal annealing

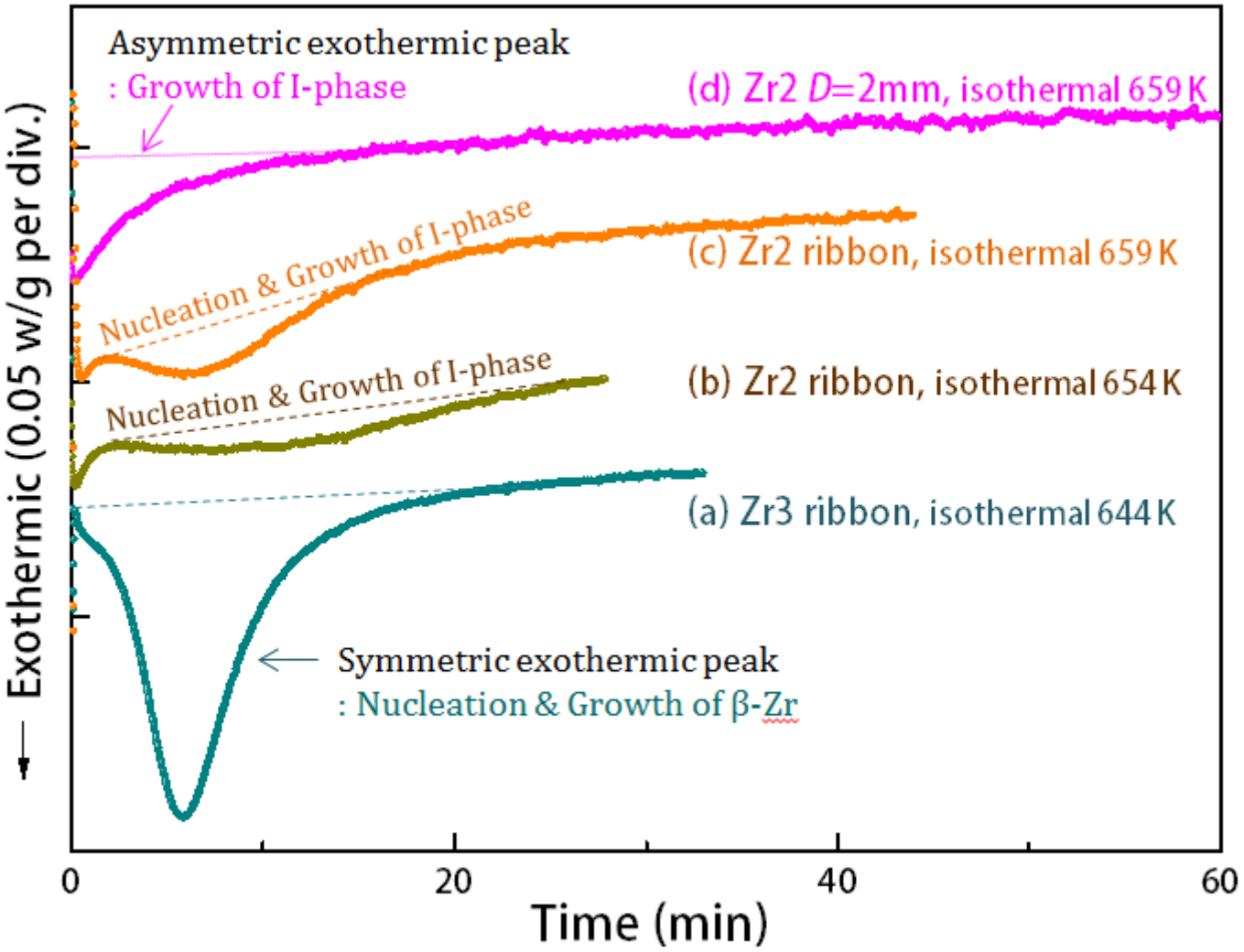

Characterizing the structure – Measurement of radial distribution function, also called pair distribution function by EXAFS analysis

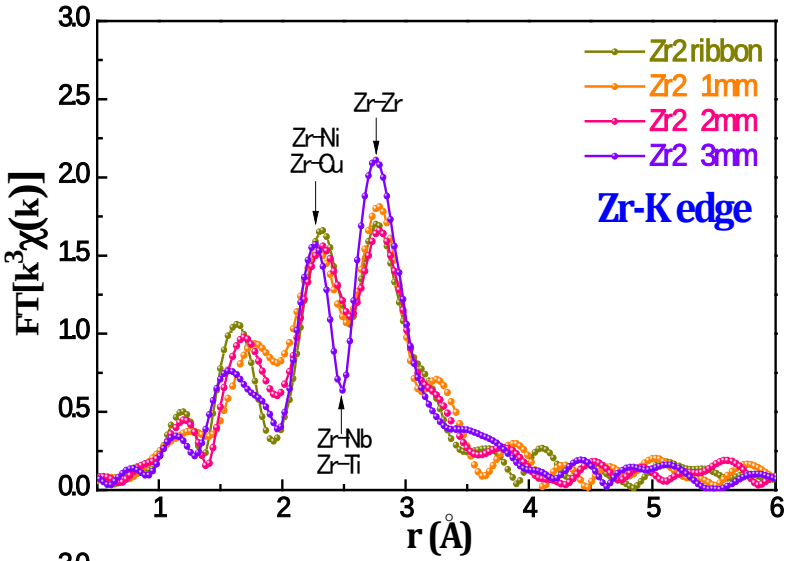

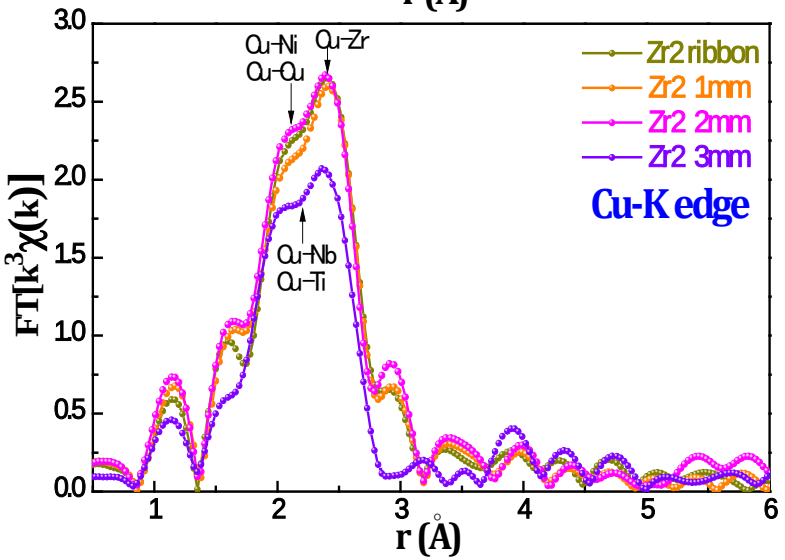

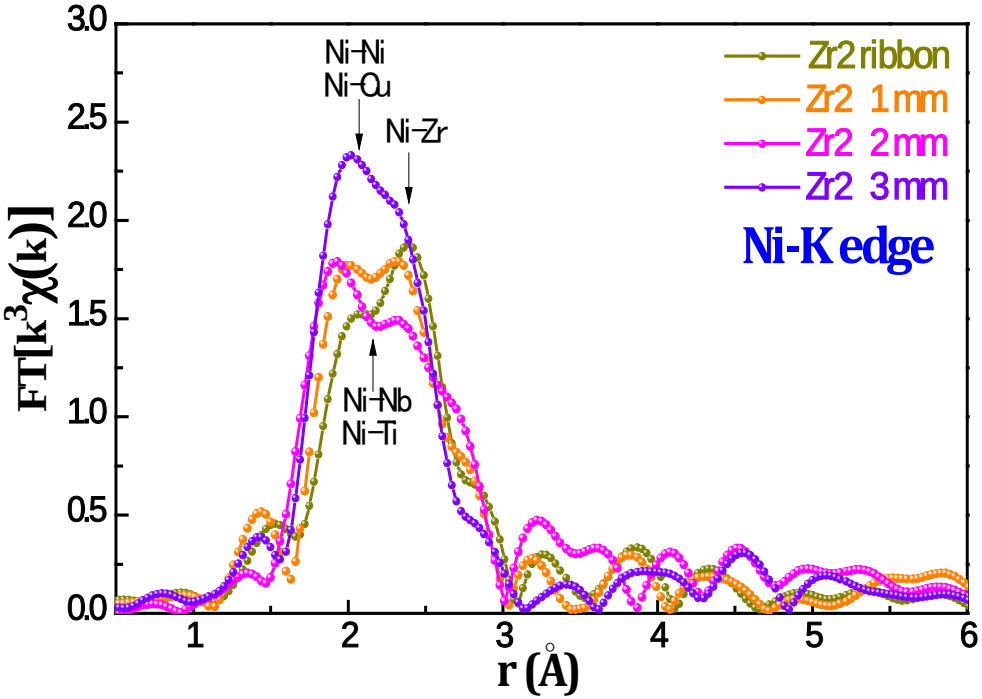

5.2.3 Structural Details

- **Amorphous vs Nanocrystalline**

1) *Microstructural observation*

XRD, (HR)TEM, *EXAFS …*

2) *Thermal analysis*

DSC (Differential Scanning Calorimetry)

: Measure heat absorbed or liberated during heating or cooling

cf) **a) *glass*** → ***nucleation & growth***

(perfect random)

b) *local clustering*: quenched-in nuclei → ***only growth***

c) *Nanocrystalline* → ***growth***

5.3 Crystallization Modes in Melt-Spun Ribbons

Variables : solid solubility, number of stable & metastable intermetallic phases, composition

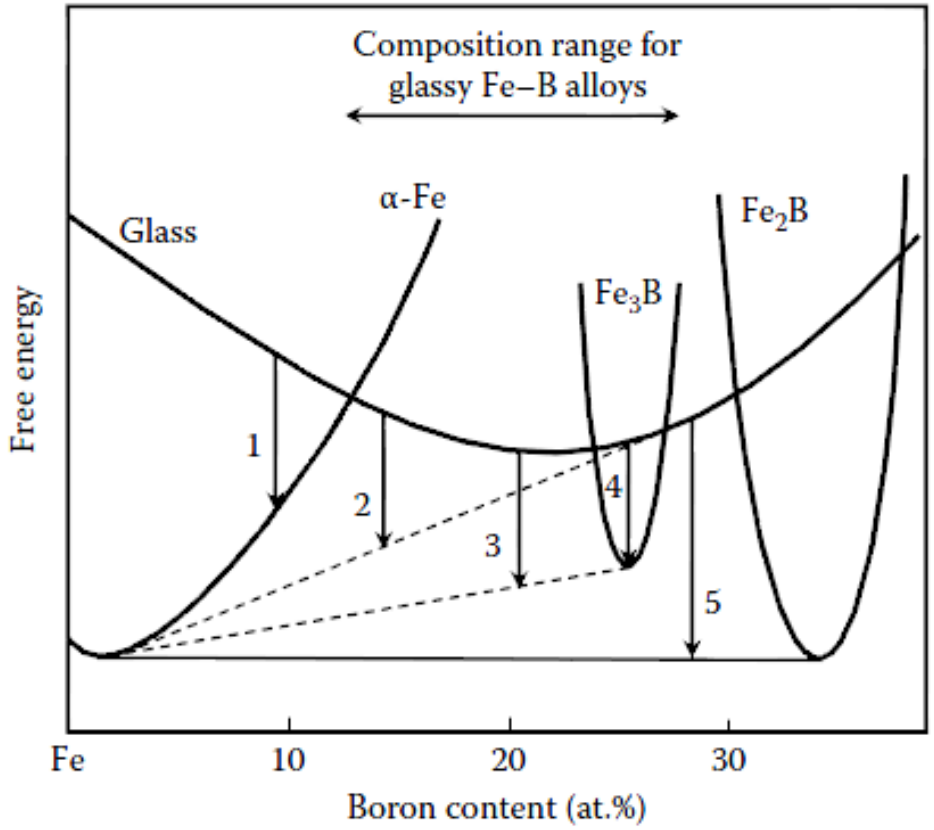

FIGURE 5.5

Hypothetical free energy vs. composition diagram for the Fe-rich Fe–B alloy system. The variation of free energy with composition is represented for the equilibrium α-Fe solid solution and the Fe_2B phases and the metastable Fe_3B phase and the glassy phase. The use of the common tangent approach will help in determining the compositions of the individual phases. The solid common tangent line represents the stable equilibrium between α-Fe and Fe_2B phases, while the dotted common tangent lines represent the metastable equilibrium between α-Fe and Fe_3B phases and α-Fe and glassy phases.

Crystallization Behaviors in Metallic Glass

Metallic glasses crystallize by a nucleation and growth process.

The driving force is the free energy difference between the glass and the appropriate crystalline phase. → (Free energy vs. Composition diagram)

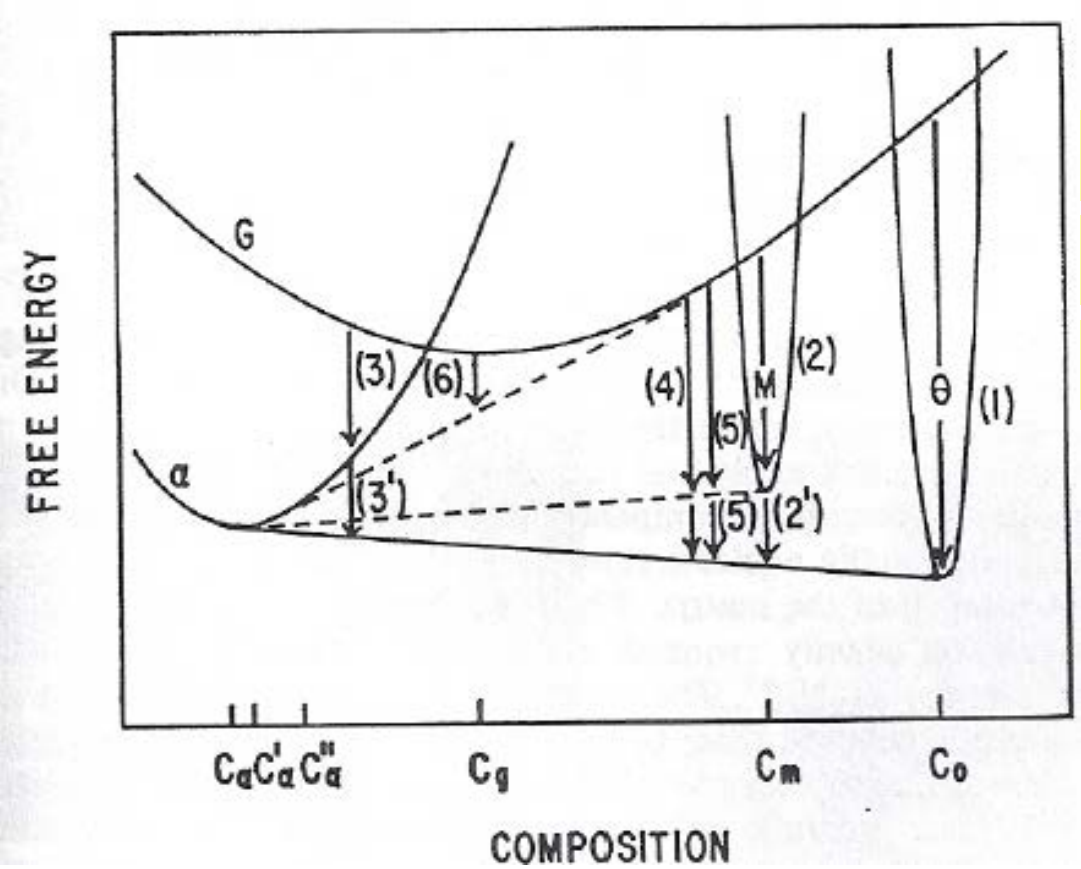

Crystallization mechanisms

1. Polymorphous Crystallization
2. Eutectic Crystallization
3. Primary Crystallization

G: Glass

α : Solid solution (Crystalline phase)

θ : Intermetallic phase

M: metastable phase

THERMODYNAMICS OF CRYSTALLIZATION

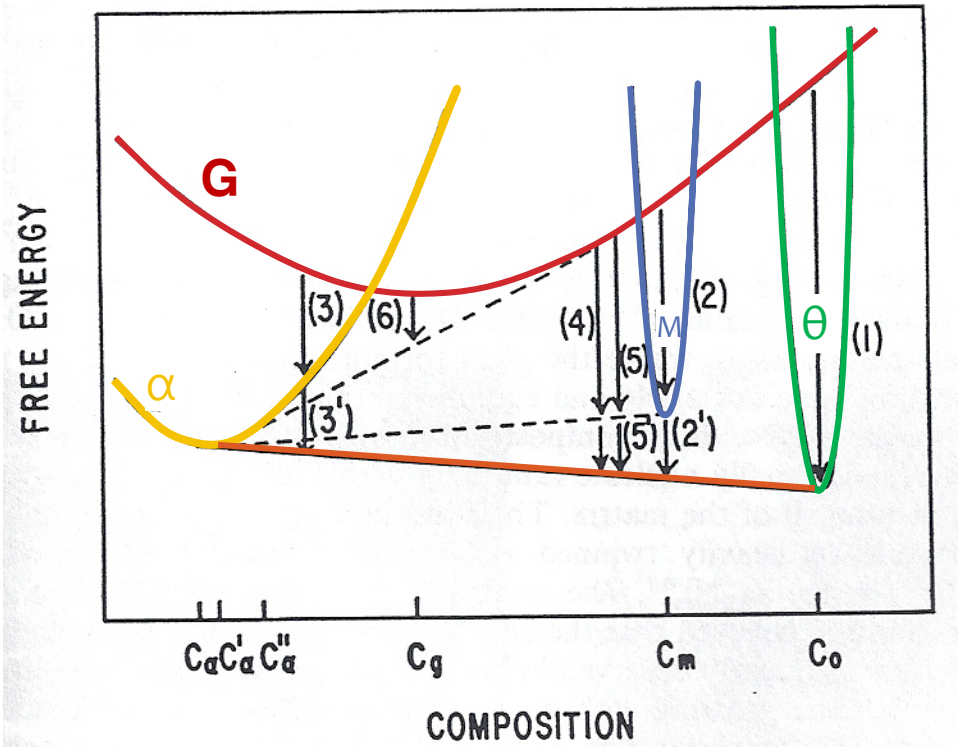

Figure 10.7 Hypothetical free energy diagram to illustrate the crystallization of a metallic glass. G, α, θ, M are respectively the free energy curves of the glass, a terminal solid solution, a stable intermetallic phase, and a metastable phase. Stable equilibrium is indicated by the solid line; metastable equilibrium by the broken lines. The numbered arrows refer to the devitrification processes described in the text

Crystallization mechanisms

(a) Polymorphous transformation of the glass to a crystalline phase of the same composition.

The product may be either θ (1) or M(2) or a supersaturated solid solution α(3).

In the latter two cases subsequent decomposition can occur to the equilibrium mixture of α and θ (2' and 3')

1. Polymorphous Crystallization: single crystalline phase without any change in composition

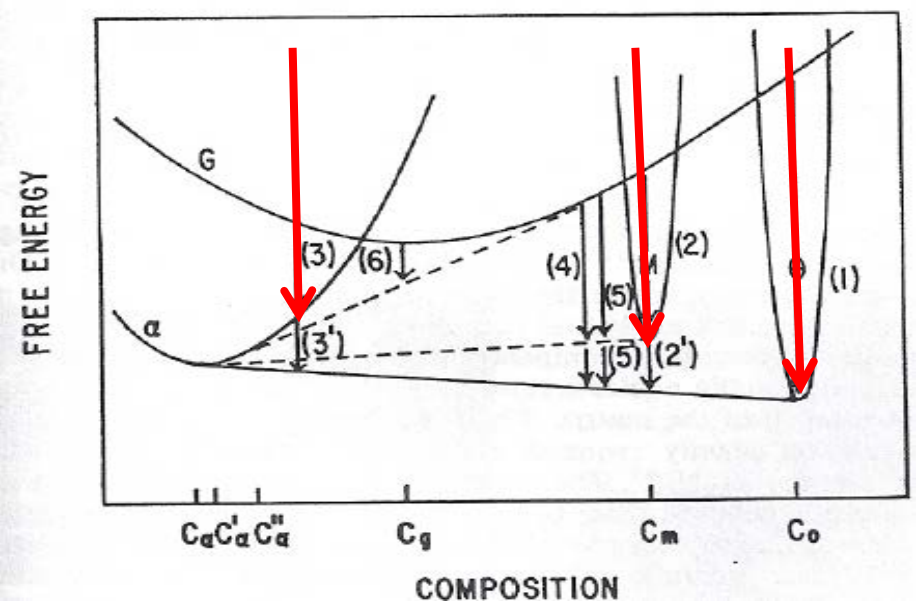

Growth rates and morphologies

$$u = a_0 \nu_0 \left\{ \exp\left[\frac{-\Delta F_a}{kT} \right] \right\} \left\{ 1 - \exp\left[\frac{-\Delta F_v}{kT} \right] \right\}$$

ΔF_a = activation energy for an atom to leave the matrix and attach itself to the growing phase

ΔF_v = The molar free energy difference btw C and G

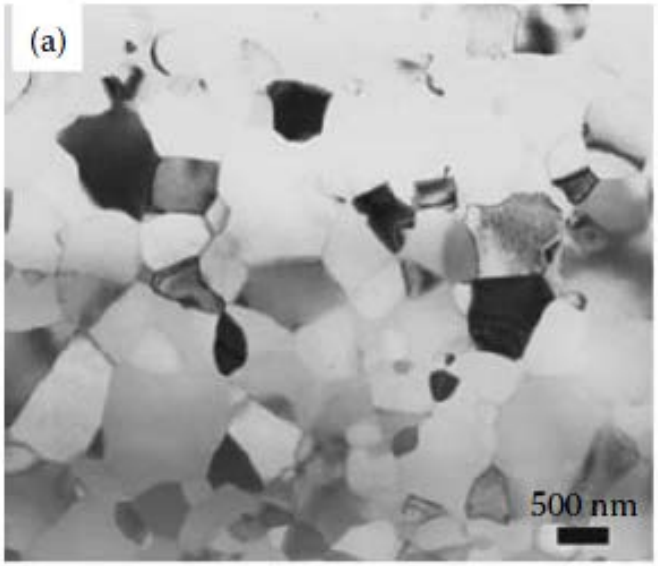

Polymorphous crystallization in a $Ti_{50}Ni_{25}Cu_{25}$ BMG alloy on annealing for 28 min at 709 K.

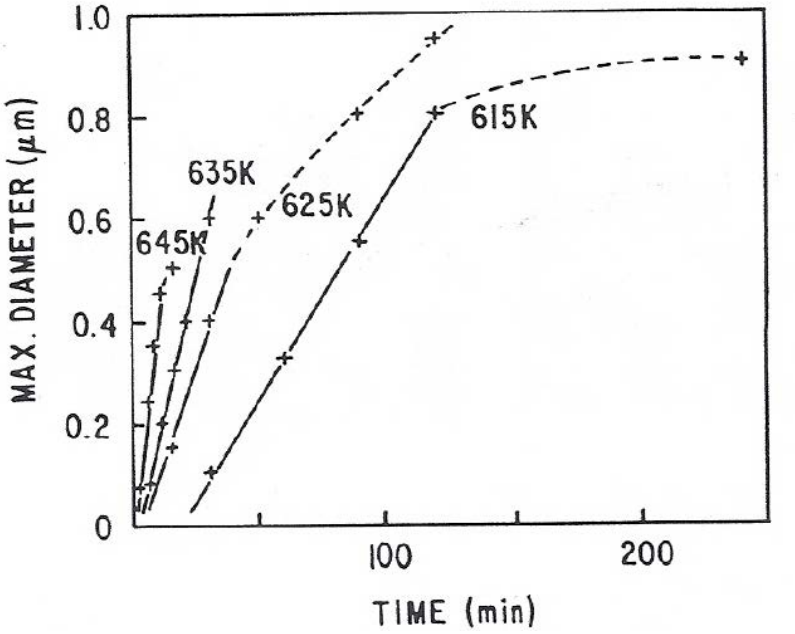

Growth kinetics of Zr_2Ni crystals in glass of same composition. The broken lines indicate crystal impingement.

THERMODYNAMICS OF CRYSTALLIZATION

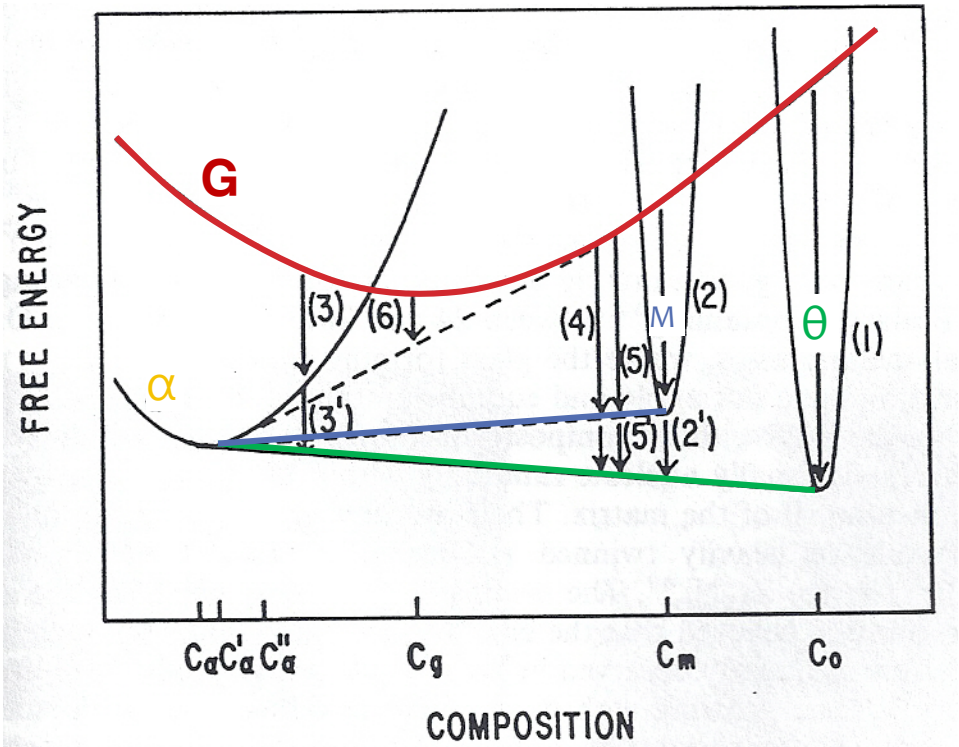

Figure 10.7 Hypothetical free energy diagram to illustrate the crystallization of a metallic glass. G, α, θ, M are respectively the free energy curves of the glass, a terminal solid solution, a stable intermetallic phase, and a metastable phase. Stable equilibrium is indicated by the solid line; metastable equilibrium by the broken lines. The numbered arrows refer to the devitrification processes described in the text

Crystallization mechanisms

(b) Eutectic crystallization of liquids

The glass can reduce its free energy to a point on the common tangent between either α and θ (4) or α and M(5).

In the case of the metastable eutectic between α and M subsequent further decomposition to α and θ can occur. (4' and 5')

2. Eutectic Crystallization

- Largest driving force
- can occur in the whole concentration range between the stable or metastable phases (Even though the whole transformation takes place in the solid state and therefore it should be more appropriately called a eutectoid crystallization, the term “eutectic” has come to stay, presumably because the stating material (the glass) is more liquid-like.)

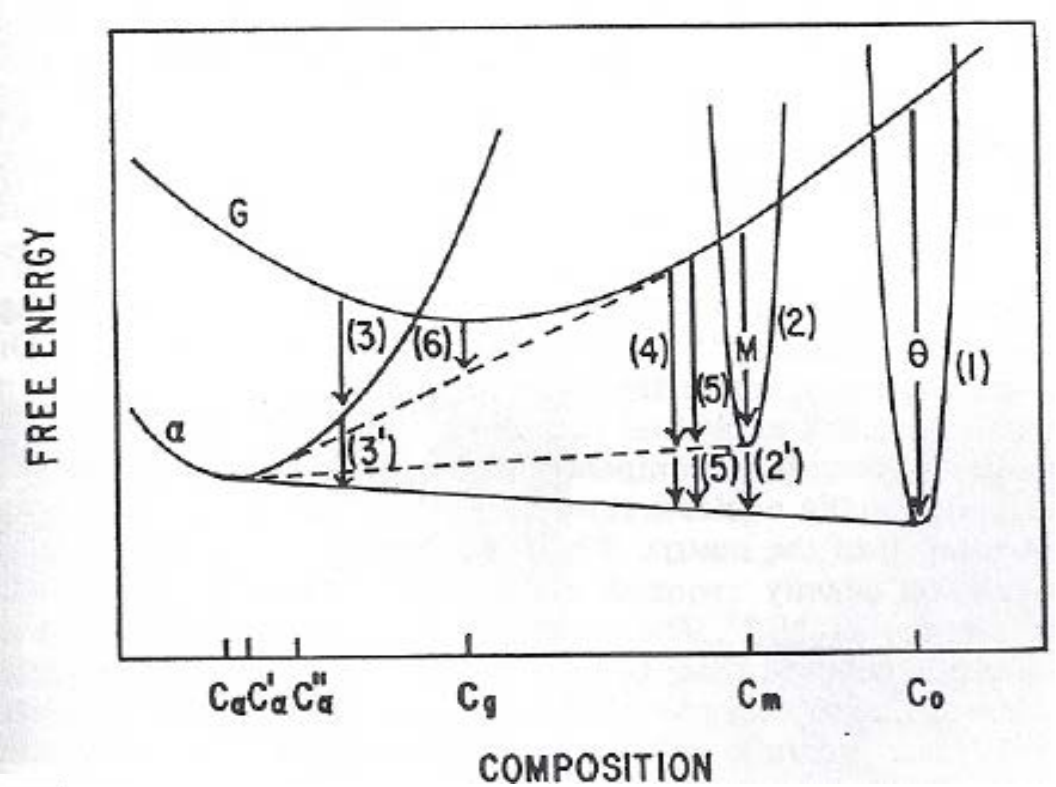

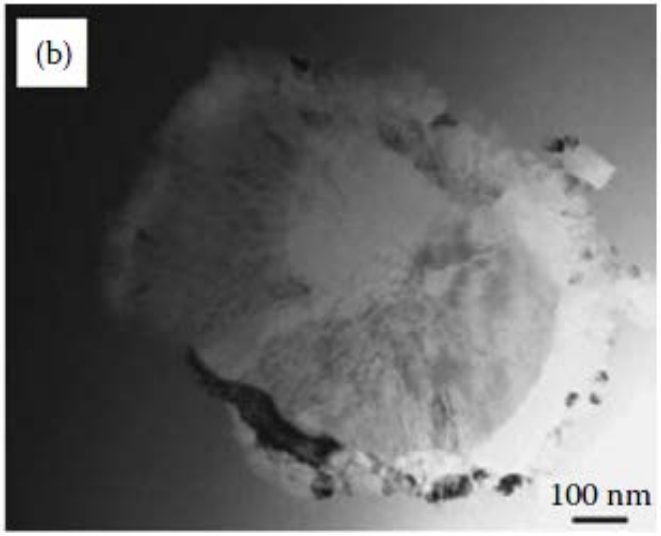

Eutectic crystallization in $Zr_{62.5}Cu_{22.5}Al_{10}Fe_5$ glassy alloy annealed for 10 min. at 713K.

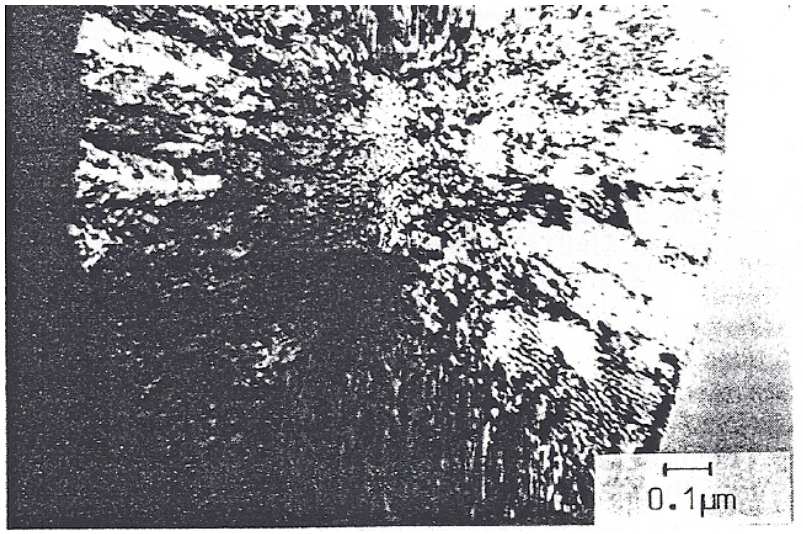

Barrel shaped eutectic crystal in $Fe_{40}Ni_{40}P_{14}B_6$ annealed for 13 min. at 385℃

THERMODYNAMICS OF CRYSTALLIZATION

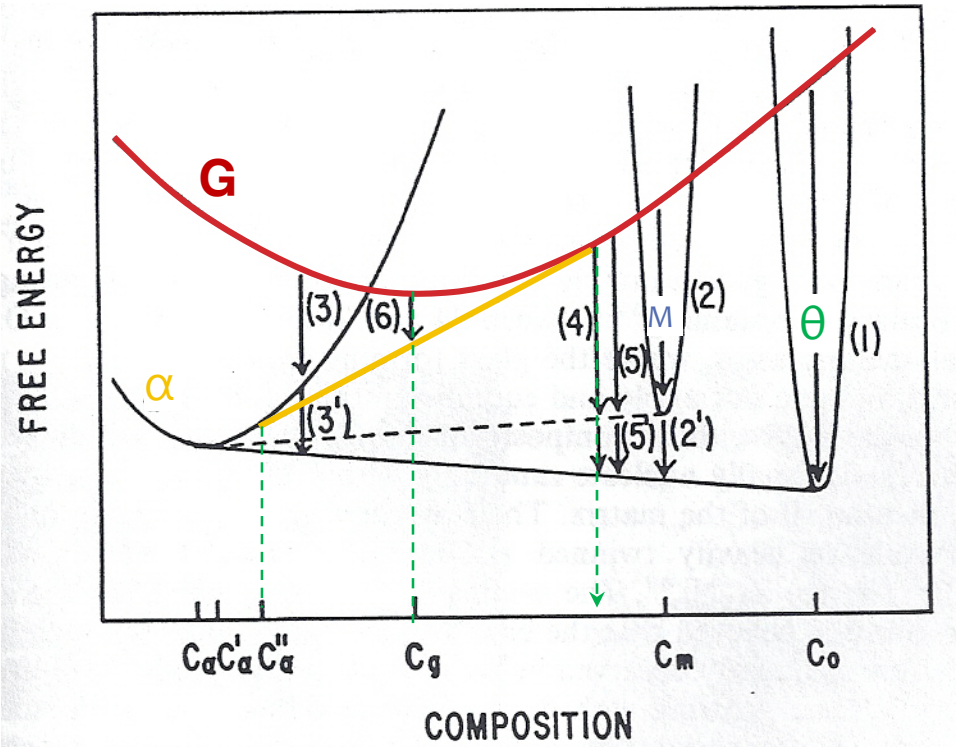

Figure 10.7 Hypothetical free energy diagram to illustrate the crystallization of a metallic glass. G, α, θ, M are respectively the free energy curves of the glass, a terminal solid solution, a stable intermetallic phase, and a metastable phase. Stable equilibrium is indicated by the solid line; metastable equilibrium by the broken lines. The numbered arrows refer to the devitrification processes described in the text

Crystallization mechanisms

(c) Primary crystallization of supersaturated solid solution (6)

Since the α has a composition c_α" which is less than that of the glass c_g solute is rejected from the growing crystals into the glass (4). Ultimately the untransformed, enriched glass (4) transforms by one of the other mechanisms discussed above.

3. Primary Crystallization

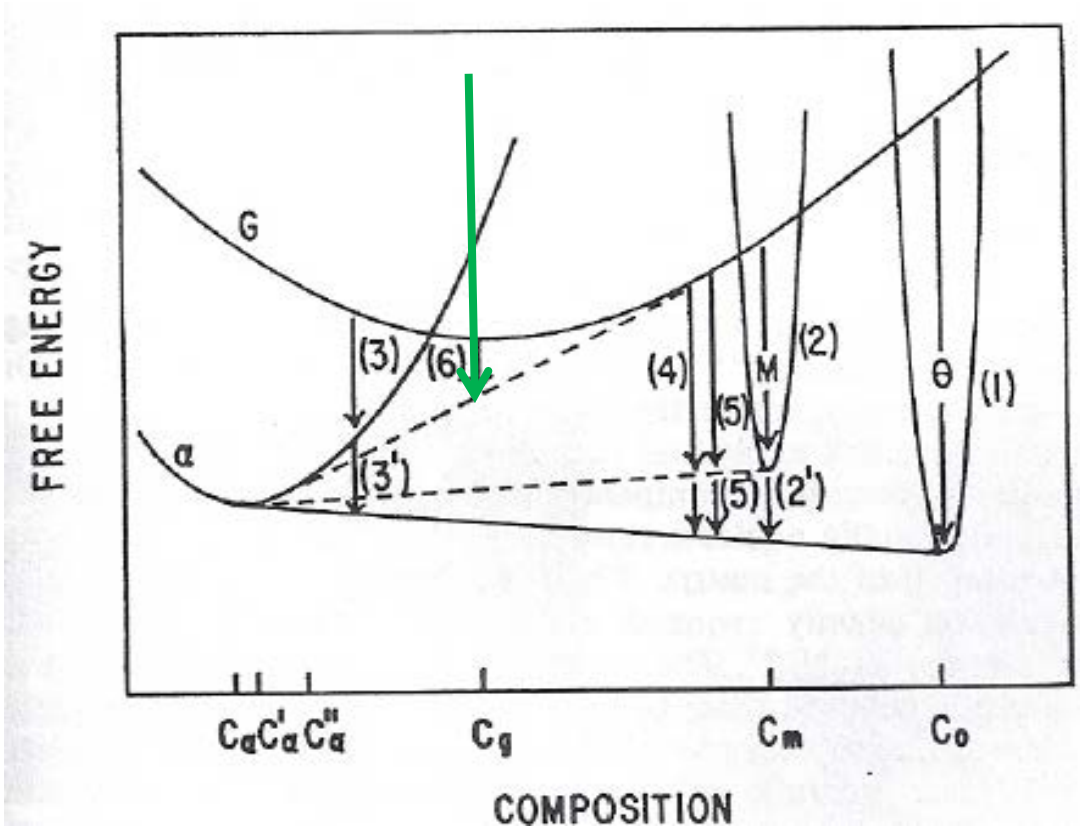

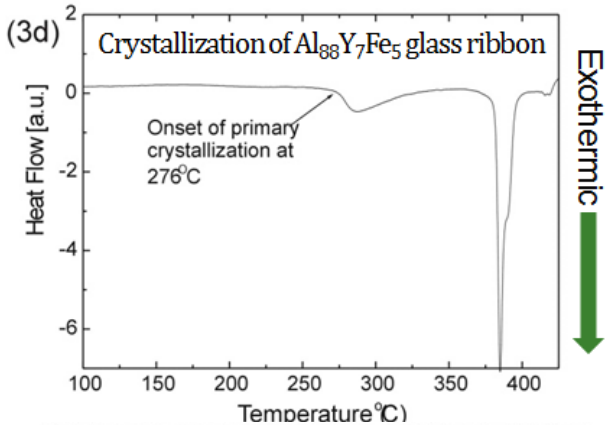

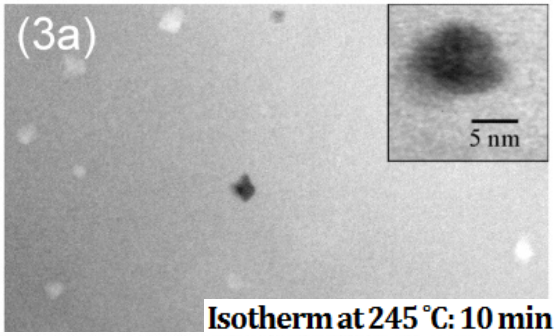

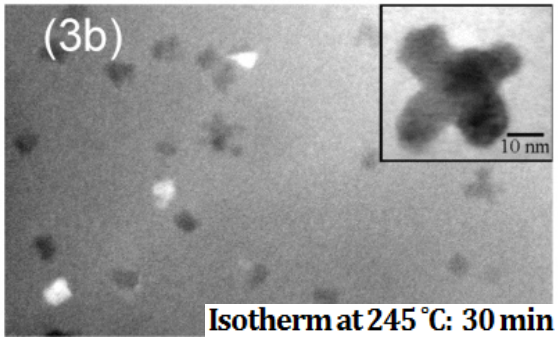

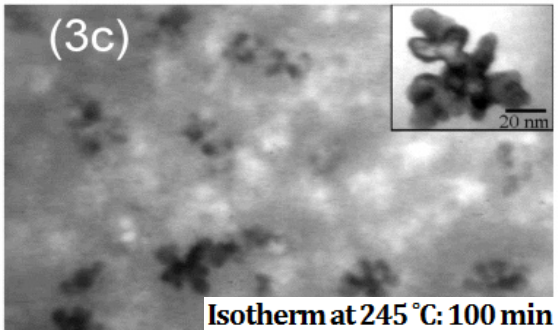

- Forms first from the glass phase
- Supersaturated solid solution
- Since the concentration of the solute in the α-Fe phase is lower than that in the glassy phase, the solute (boron) atoms are rejected into the glassy phase and consequently the remaining glass phase becomes enriched in B until further crystallization is stopped.

Thermodynamics of Crystallization

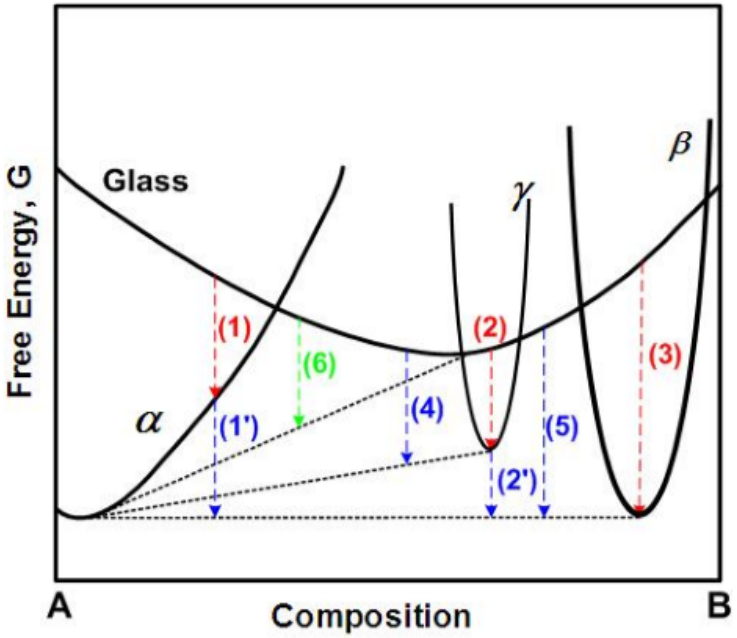

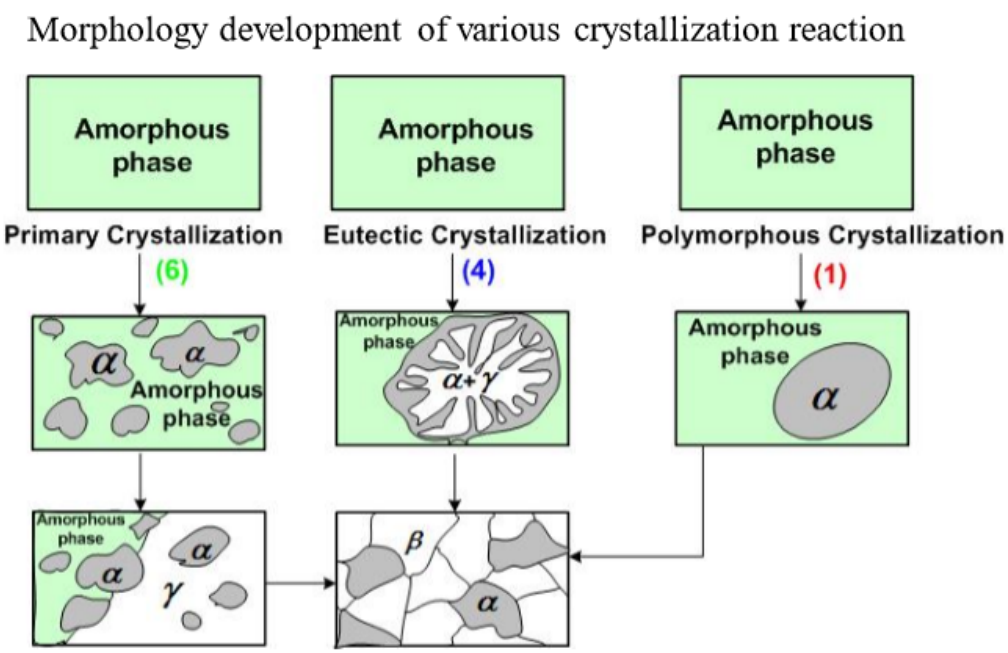

Polymorphous crystallization (1) $Am_1 \rightarrow \alpha$

Eutectic crystallization (4) $Am_1 \rightarrow \alpha+\gamma$

Primary Crystallization (6) $Am_1 \rightarrow \alpha+Am_2$

5.5. Thermal Stability of Metallic Glasses

(a) Variation of T_g and T_x in the $Zr_{65}Al_xCu_{35-x}$ (x=0, 7.5, 20) alloys

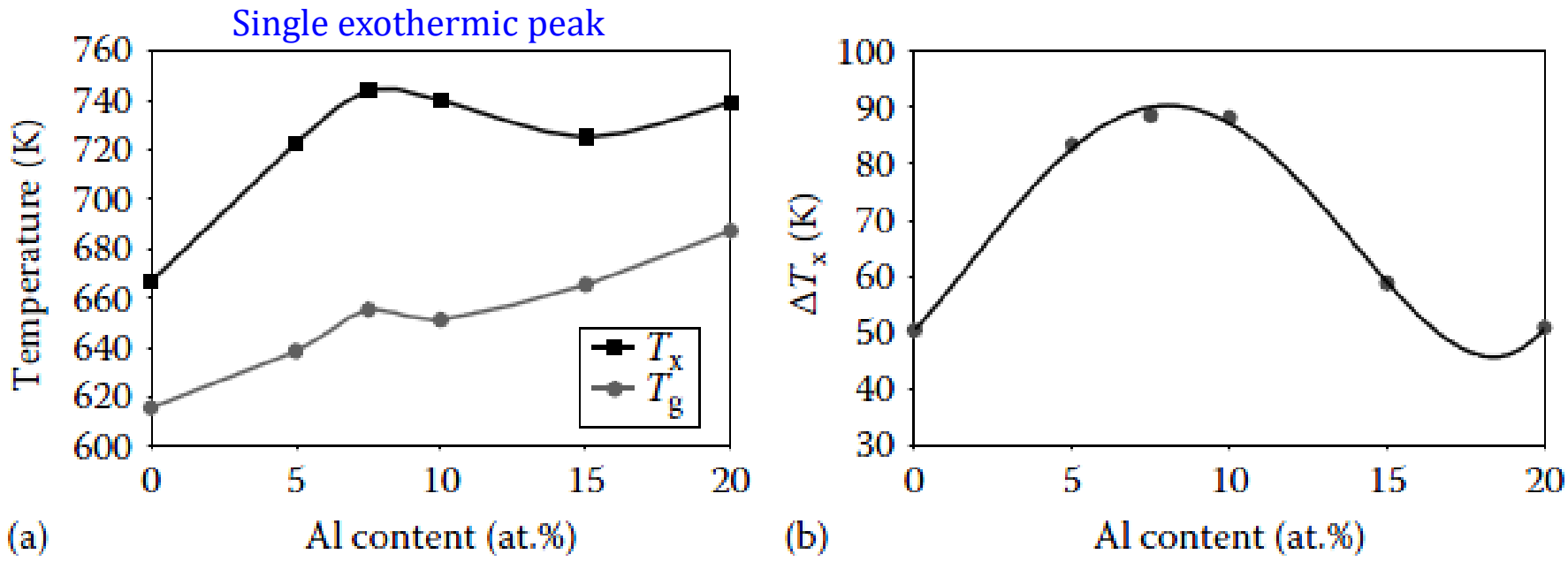

FIGURE 5.7
Variation of (a) T_g and T_x temperatures, and (b) the width of the supercooled liquid region ΔT_x (= $T_x - T_g$), with Al content in the $Zr_{65}Al_xCu_{35-x}$ glassy alloys. (Reprinted from Inoue, A. et al., *Mater. Sci. Eng. A*, 178, 255, 1994. With permission.)

5.6. Crystallization Temperatures and Their Compositional Dependence

Compositional dependence.

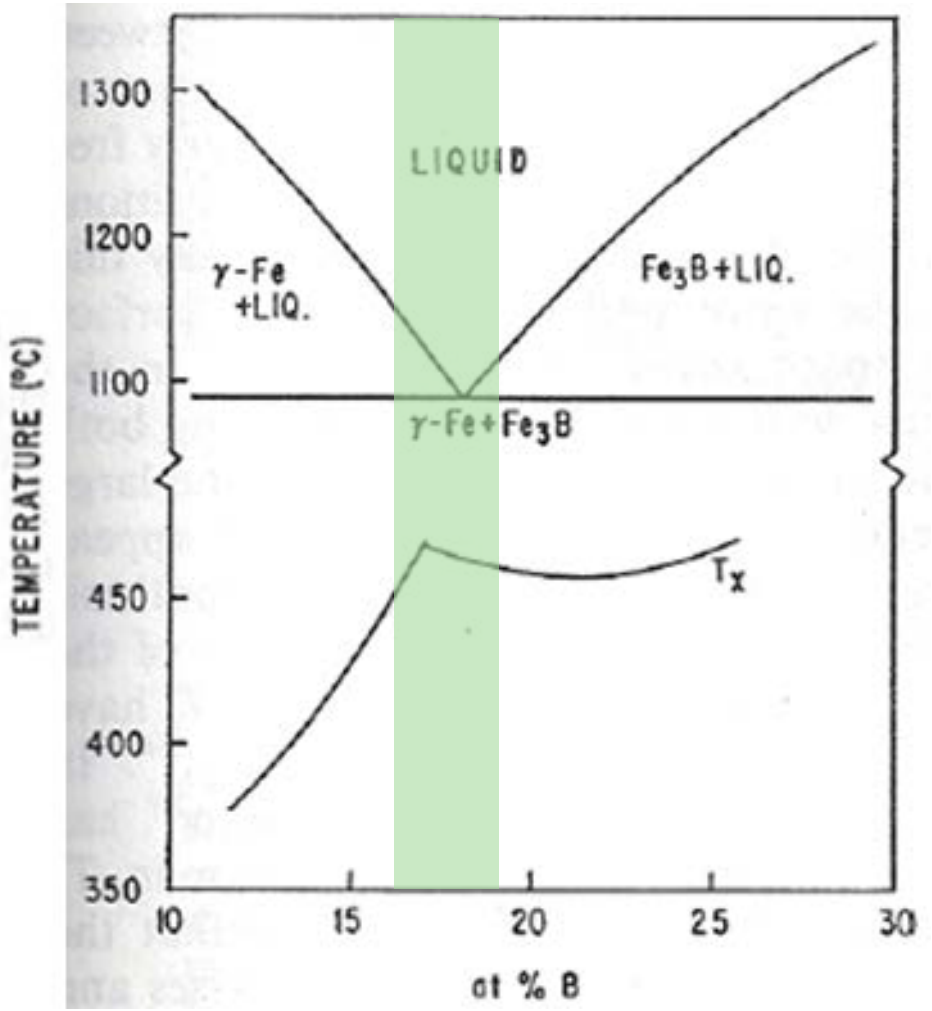

In many binary

Metal-Metalloid glass (Fe-B)

T_x is a maximum near the eutectic composition

→ The same does not appear to be the case in all-metallic glasses

Metal-Metal glass (Ni-Zr)

A monotonic decrease of T_x with increasing Zr content despite the existence in two eutectics

5.6. Crystallization Temperatures and Their Compositional Dependence

Compositional dependence.

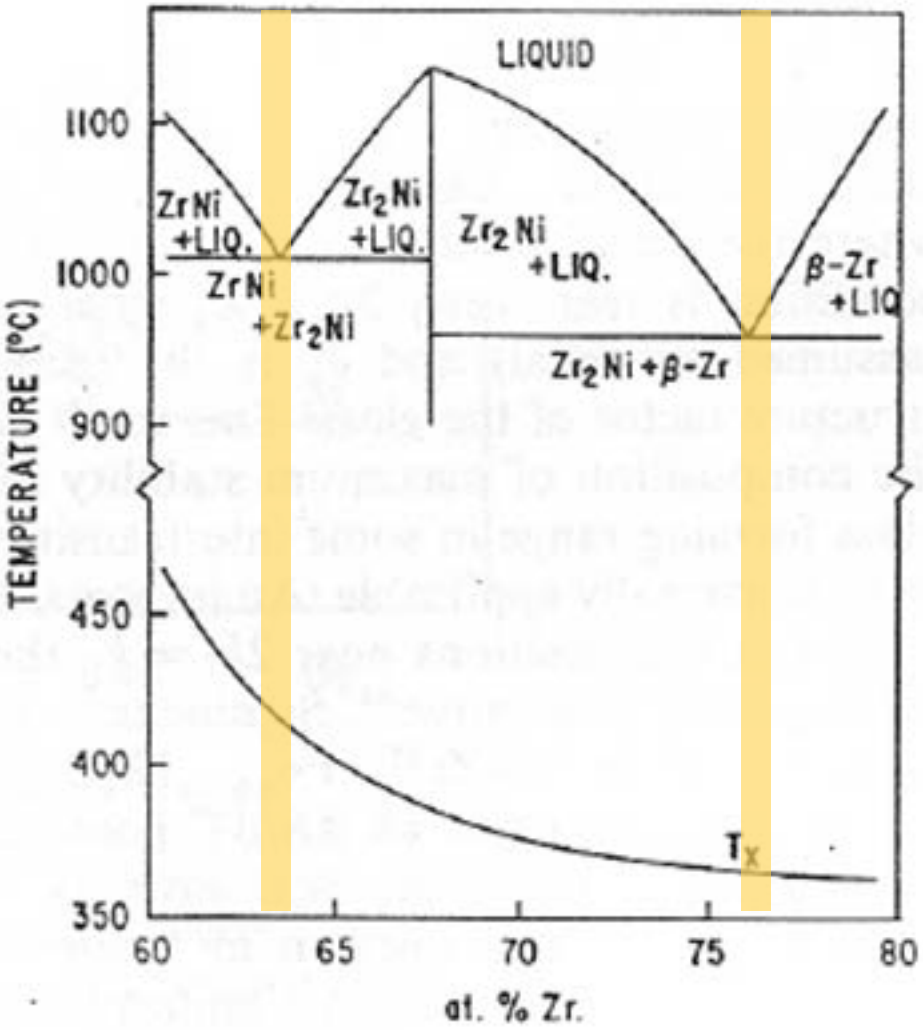

In many binary

Metal-Metalloid glass (Fe-B)

Tx is a maximum near the eutectic composition

→ The same does not appear to be the case in all-metallic glasses

Metal-Metal glass (Ni-Zr)

A monotonic decrease of T_x with increasing Zr content despite the existence in two eutectics

5.5. Thermal Stability of Metallic Glasses

(b) Arrhenius plot of the incubation time for the precipitation of crystalline phases (τ) in the $Zr_{65}Al_xCu_{35-x}$ (x=0, 7.5, 20) alloys

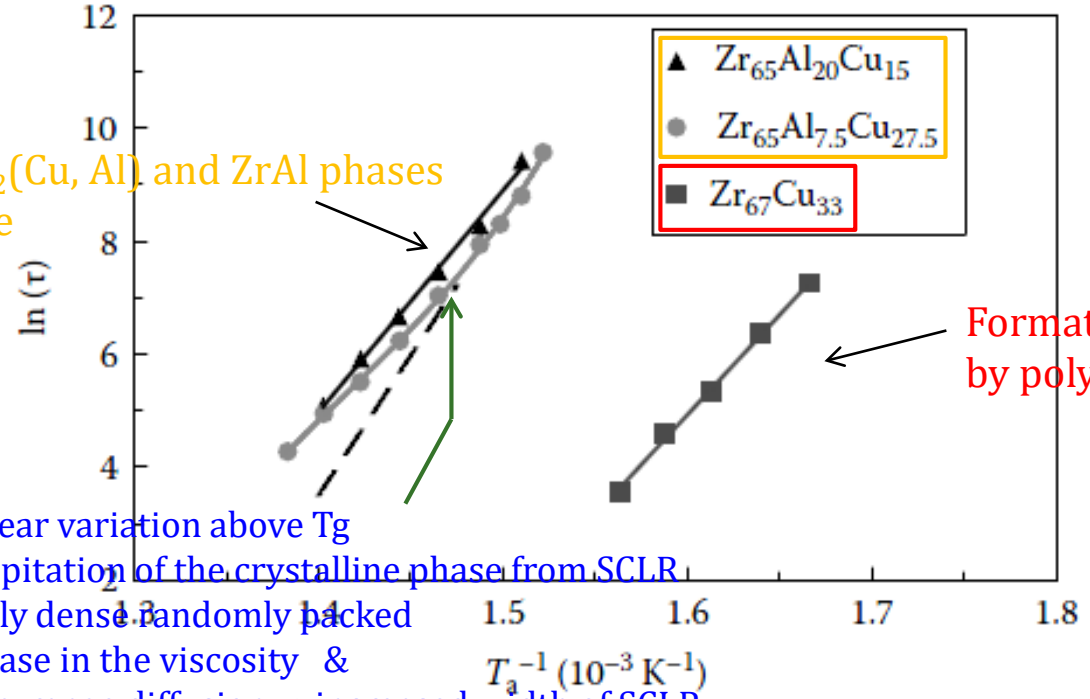

$$\tau \propto \frac{T\eta}{(T_\ell - T)^2}$$

Formation of $Zr_2(Cu, Al)$ and ZrAl phases by eutectic mode

Formation of Zr_2Cu phase by polymorphous mode

Shifted from the linear variation above Tg
→ suppressed precipitation of the crystalline phase from SCLR due to possess highly dense randomly packed structures → increase in the viscosity & difficult to have long-range diffusion → increased width of SCLR

FIGURE 5.8
Arrhenius plot of the incubation time, τ for the precipitation of crystalline phases in the binary $Zr_{67}Cu_{33}$, and ternary $Zr_{65}Al_{7.5}Cu_{27.5}$ and $Zr_{65}Al_{20}Cu_{15}$ alloys. Note the deviation of τ to the positive side of the linear variation (to higher temperatures) only for the ternary $Zr_{65}Al_{7.5}Cu_{27.5}$ alloy, signifying the delayed crystallization in the alloy with 7.5 at.% Al. Such a deviation is not observed for the other alloys. (Reprinted from Inoue, A. et al., *Mater. Sci. Eng. A*, 178, 255, 1994. With permission.)

(C) Annealing up to T_a at a heating rate of 0.17 K/s (10K/min), annealed there for 60s
→ measure peak temperatures for the nucleation and growth reactions of the crystalline phases in the $Zr_{65}Al_xCu_{35-x}$ (x=0, 7.5) alloys

* Difference in the reciprocals of the Tp between the Pre-annealed and as-quenched samples

688 K, correspond to the peak temp. of the nucleation event of a crystalline phase formation

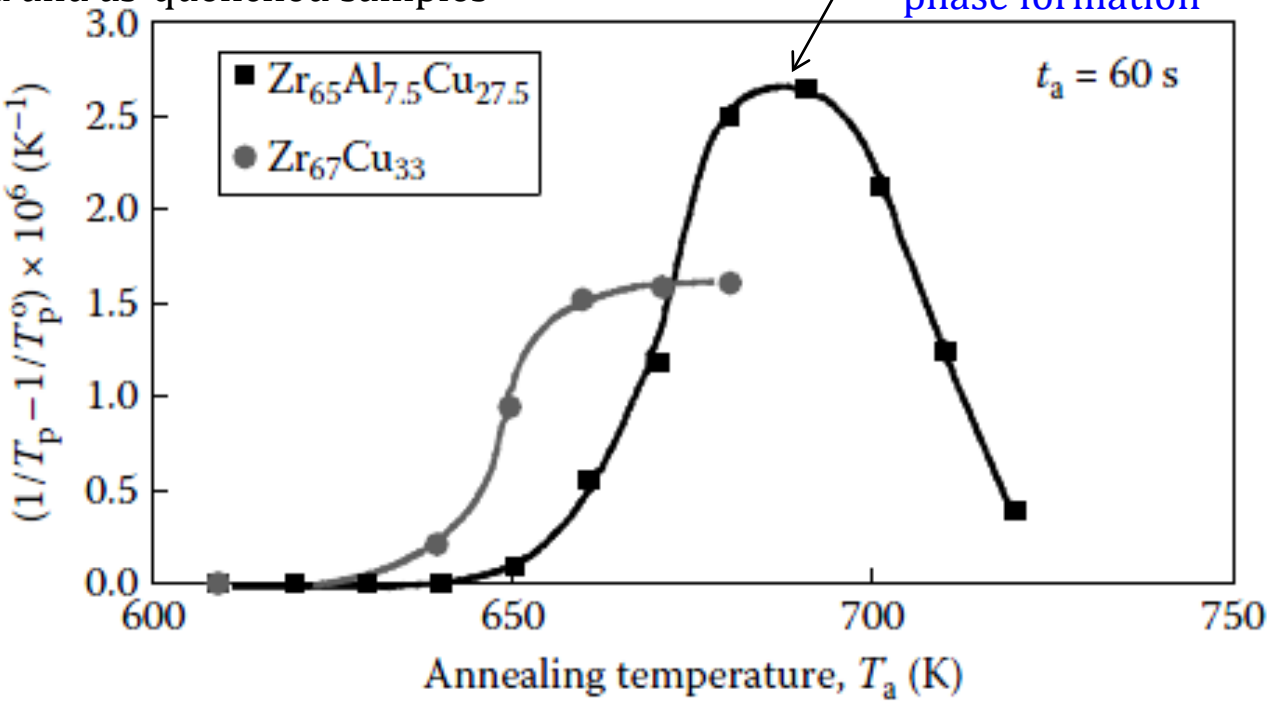

* Measure Tx at a very high heating rate of 5.33 K/s (320 K/min) = corresponding to the maximum growth rates, that is growth temperature
- Zr67Cu33: Just above the maximum temp of 670 K/ difference ~ very small
- Zr65Al7.5Cu27.5: the difference btw max nucleation and max growth temp. ~143K, resulting in enhanced resistance to crystallization (high thermal stability)

* Heating rate ↑ – not significantly increase the grain size in Zr67Cu33 ↔ considerably large grain size in Zr65Al7.5Cu27.5 due to the presence of fewer nuclei

5.7. Annealing of Bulk Metallic Glasses: SR → SCLR (& PS) → Crystallization

Figure 5.11 Different pathways for a metallic glass to crystallize into the equilibrium phases